R. & M. No. 3639

R. & M. No. 3639

MINISTRY OF TECHNOLOGY

AERONAUTICAL RESEARCH COUNCIL
REPORTS AND MEMORANDA

Low-Speed Wind-Tunnel Tests on a Wing Section with Plain Leading- and Trailing-Edge Flaps having Boundary-Layer Control by Blowing

By J. A. LAWFORD and D. N. FOSTER
Aerodynamics Dept., R.A.E., Farnborough

LONDON: HER MAJESTY'S STATIONERY OFFICE
1970
PRICE 18*s.* 0*d.* [90*p.*] NET

Low-Speed Wind -Tunnel Tests on a Wing Section with Plain Leading- and Trailing-Edge Flaps having Boundary-Layer Control by Blowing

By J. A. LAWFORD and D. N. FOSTER
Aerodynamics Dept., R.A.E., Farnborough

Reports and Memoranda No. 3639*
April, 1969

Summary.

Low-speed wind-tunnel tests have been made, under as near two-dimensional conditions as possible, on a wing section with plain leading- and trailing-edge flaps. The increases of lift resulting from boundary-layer control by blowing over the trailing-edge flap have been measured for a range of flap deflections, as has the effectiveness of a leading-edge flap for increasing the stalling incidence and maximum lift coefficient.

Some comparisons with the predictions of inviscid theory have shown good agreement between predicted and measured pressure distributions, and suggest that minimum aerodynamic drag occurs when the inviscid lift is achieved.

LIST OF CONTENTS

*Replaces R.A.E. Technical Report No. 69 078—A.R.C. 31 371.

LIST OF CONTENTS—*continued*

---

1. *Introduction.*

The use of boundary-layer control by blowing over flaps, to achieve high lift, has been the subject of a number of experiments and reviews[1]. The major part of the existing data is on swept wings of small to moderate aspect ratio, and there was therefore a need for data which might be applicable to large aspect ratio wings. This Report gives the results of tests on a wing with plain flaps, having boundary-layer control by blowing, mounted between the roof and floor of a wind tunnel. Special techniques, involving control of the roof and floor boundary layer by distributed suction, were employed to ensure two-dimensional conditions. The experimental technique, and the effect on the wing spanwise load distribution, have been separately reported[2].

The purposes of these tests were:

(i) To obtain basic sectional data on the behaviour of leading- and trailing-edge plain flaps with boundary-layer control by blowing, and (ii) to compare experimental results with calculations for inviscid flow, and to relate the measured behaviour of the boundary layer to the blowing momentum.

In this Report, the experimental results and comparisons with the results of inviscid flow calculations are given.

2. *Description of the Model and Rig.*

2.1. *The Model.*

A section of the wing is shown in Fig. 1. A chord of 4 ft (1·22 m) was determined by general design considerations for the other tests for which this wing was used[3]. It was of RAE 102 section, of thickness/chord ratio 0·13, with an $a = 0{\cdot}4$ camber line for $C_{L_{opt}} = 0{\cdot}2$. Co-ordinates for the section with undeflected flaps are given in Table 1. Two plain hinged flaps were provided, the hinges being on the wing lower surface. The leading-edge flap/chord ratio was 12·5 per cent, and the trailing-edge flap/chord ratio 25 per cent. The trailing-edge flap hinge allowed slight adjustment normal to the chord-line, and for almost all the tests the position set was such that the jet sheet blew tangential to the flap surface, with a downward 'step' of 0·06 in (0·15 cm) from the shroud upper surface to the flap surface. This step was faired by adhesive tape for some tests without trailing-edge flap blowing; for one of these a higher flap position, giving a faired step of 0·025 in (0·06 cm) was used. The forward blowing slot was faired except when blowing at the

leading-edge flap was used. Transition was free throughout the test series.

Nozzles were installed to blow at the leading-edge flap knee and at the trailing-edge flap shroud; slot depths were 0·028 in (0·071 cm) and 0·042 in (0·107 cm) respectively. The blown span was 9 ft (2·74 m); the nozzles were each in three sections of 3 ft (0·91 m) span, and were fed with air through six spanwise ducts, each supplying one nozzle section through six main feed pipes to a spanwise plenum chamber, and thence through connector ducts to a final plenum chamber and then to the slot. A reference pressure was measured in each nozzle section at the final plenum chamber.

Static pressure tappings were provided at a section close to the wing mid-span; the number of points varied between 62 and 68 depending on the flap deflection. Tufts on the flap and wing upper surfaces were used for visual assessment of the flow behaviour.

2.2. *The Rig.*

The wing was mounted in the 13ft × 9ft low-speed wind tunnel of the British Aircraft Corporation at Weybridge, spanning the 9ft vertical dimension of the tunnel between turntables in the roof and floor. A schematic diagram of the rig is shown in Fig. 2, and a photograph in Fig. 3. In order to minimise interference effects on tunnel speed and static-pressure calibration due to circulation round the model at high lift[4], a tunnel reference pressure tapping was fitted in the floor, in the plane of the wing chord at zero incidence, and in the same transverse plane as the usual wall tappings at the downstream end of the contraction; this tapping was calibrated against the wall tappings with the tunnel empty, and was used to obtain tunnel speed and static pressure during the tests.

Air from the compressor passed into a plenum chamber, and thence into six separate supply lines leading to each of the six spanwise model ducts. Each line consisted of a valve, a venturi measuring the flow rate in the line, and a flexible tube connected to the model duct.

The tubes from the wing pressure tappings, and the tunnel floor reference tapping, were connected to three scanivalves, and thence to pressure transducers; transducers with ranges of ± 1 lb/in^2, $\pm 2{\cdot}5$ lb/in^2 and ± 5 lb/in^2 (7 KNm^{-2}; 17 KNm^{-2} and 34 KNm^{-2} respectively) could be connected to each scanivalve as test conditions required. The accuracy of the transducers was $\pm\frac{1}{4}$ per cent of the maximum pressure.

Two rakes of pitot tubes for boundary-layer measurements were fitted on the wing adjacent to the pressure measurement station but sufficiently removed to avoid interference. These were on the upper surface, 0·041 chord forward of the blowing slot and on the flap 0·018 chord forward of the trailing edge, measured along the surface. Both rakes had tubes for measurement of static pressure. Pressures from the rakes were read by a scanivalve and transducer with a range of ± 1 lb/in^2 (7 KNm^{-2}). Boundary-layer measurements were taken also on the wing upper surface (0·422c) and near the blowing slot (0·725c) by traversing a remotely operated pitot or static tube through the boundary layer. This was done at a few conditions only.

The momentum in the wake downstream of the model was measured by a rake mounted at the centreline height of the model, and approximately one chord downstream of the model. The rake consisted of 37 pitot tubes, spaced 0·5 inch ($\simeq$ 0·01 chord) apart, and 10 static tubes, these being adjacent to every fourth pitot tube. The rake was mounted such that it could be moved normal to the airstream, and it was also possible to rotate it about the centre pitot tube to align it with the wake.

3. *Description of Tests.*

3.1. *Calibration of Nozzles.*

Before the wind-tunnel tests, each section of the blowing nozzles was individually calibrated away from the model. Traverses along each slot showed rapid variation of stagnation pressure, peak values occurring at the positions of the connector ducts into the final plenum chamber. Fig. 4 shows a typical stagnation pressure distribution over a six inch length of the central trailing-edge nozzle.

Each nozzle section was calibrated by the following method. Stagnation pressure measurements were taken in close traverses (every 0·1 inch) along the slot at two reference pressures, and in more widely spaced traverses (every 1·0 inch) at about 15 reference pressures covering the range for which the nozzles were designed. Mass flow rate measurements were obtained by an orifice plate. A mean ratio of stagnation

pressure to reference pressure was obtained for each traverse, and these ratios were plotted against reference pressure. It was then assumed that the ratios derived from the closely spaced traverses were correct for the relevant reference pressure, and that the widely spaced traverses, although in error because fewer points had been taken, showed correctly the variation of the ratio with reference pressure. The results of the widely spaced traverses were multiplied by a factor varying linearly with reference pressure so as to give the correct ratios for the closely spaced traverses, to obtain the final variation by mean stagnation pressure with reference pressure. By assuming adiabatic expansion from the mean stagnation pressure to free stream static pressure and using the measured mass flows, values of blowing momentum coefficient for a given reference pressure were obtained at the test conditions.

3.2. *Wind-Tunnel Tests.*

Pressure measurements at the centreline station were taken at the range of conditions tabulated in Table 2; at most of these boundary-layer measurements by the fixed rakes were also taken, although in a few instances malfunctioning of the equipment prevented this. Drag measurements by the wake rake were taken at a smaller number of conditions, indicated by an asterisk in Table 2. The primary variables were trailing-edge flap angle and the blowing quantities, the nose flap setting being used to control stalling at the leading edge; the trailing-edge flap settings of 0° and 20° were tested with the nose flap at 0° only (apart from one unblown case with trailing-edge flap at 0°), and with trailing-edge flap at 60° the leading-edge flap was at 30° only. Leading-edge flap settings of 0° and 30° were used with the trailing-edge flap at 40°.

The wind speed for the tests (except where otherwise stated) was 149 ft/s (44·8 ms^{-1}), giving a Reynolds number based on wing chord of $3{\cdot}78 \times 10^6$.

For each condition the required blowing momentum was set by adjusting the line valves to give the nozzle reference pressures indicated by the calibrations. The momentum coefficient was calculated in each case from measurements of mass flow, reference pressure, and barometric pressure taken during the test; values of C'_μ so obtained agreed well with the calibration values.

At each condition of flap setting and blowing momentum the roof and floor suction controlling the tunnel boundary layer was adjusted to give a uniform stall across the span; this suction level was maintained at all incidences.

4. *Results and Discussion.*

4.1. *Calculation Methods.*

A correction to wind speed for blockage due to the model was applied[5], and measured pressures on the wing were then converted to pressure coefficients (C_p). Integration round the centreline section gave force and moment coefficients, and corrections for the effect of tunnel constraint were applied to these and to incidence[5]. The ratio of wing chord to tunnel dimension normal to the wing being fairly large (0·31), these corrections were significant; typical values of correction to C_L, adjusted to a fixed incidence to indicate the effect on a plot of C_L *vs.* α, range from $+0{\cdot}02$ at low incidence and flap angle to $-0{\cdot}17$ at high incidence and flap angle. Where measured pressures indicated flow separation from the flap upper surface a correction for wake blockage was applied to tunnel speed[5] and hence to the force and moment coefficients.

Values of drag coefficients were derived from the wake rake measurements by the method of Ref. 6. (The distribution of pressure points at the centreline did not permit accurate integration in the drag sense.) The span of the rake (18 in, (45·7 cm)) limited measurements to conditions where the flow was sensibly attached to the flap.

Measurements in the boundary layer by the rakes fitted to the surface gave distributions of velocity within the layer, and from these values of displacement and momentum thicknesses were derived. Velocity profiles at high incidence, particularly downstream of the blowing slots, did not always converge to constant values within the rake height, and displacement and momentum thicknessess could not be obtained in these cases.

4.2. *Results.*

4.2.1. *Lift.* Curves of lift coefficient against incidence for the range of flap angles and blowing quantities are plotted in Figs. 5 to 13. Fig. 5 shows the small effect of movement of the undeflected trailing-edge flap normal to the chord-line with the slot faired, and of fairing the slot. Fig. 6 shows the effect of Reynolds-number variation with undeflected flaps and blowing slots sealed: up to an incidence of 8° and lift coefficient of 1·0 there is little effect; at higher incidence there is lift loss and earlier stall at low Reynolds number, but above a value of $3{\cdot}78 \times 10^6$ change of R has little effect. (Reynolds number was varied by change of wind speed, with consequent change of Mach number; the highest Mach number was less than 0·2 so effects due to this would be insignificant.) These tests, plotted in Figs. 5 and 6, were made without tunnel-wall suction. Fig. 7 shows that suction at this flap setting has little effect on lift coefficient*. For all subsequent figures, suction has been used to achieve as near two-dimensional conditions as possible.

Fig. 8 to 13 show for the different flap settings the increases in lift coefficient which were obtained by blowing at the trailing- and leading-edge flaps, a maximum value of over 5·7 being achieved with trailing-edge flaps at 60° and leading-edge flap at 30°, using blowing at the trailing-edge flap only at a $C'_{\mu R}$ of 0·113, or using leading-edge blowing with $C'_{\mu N} = 0{\cdot}025$ in conjunction with trailing-edge flap blowing at $C'_{\mu R} = 0{\cdot}09$ (the total blowing momenta being therefore almost equal in the two cases). Fig. 11 shows, for a trailing-edge flap angle of 40°, the beneficial effect of controlling the leading-edge separation by drooping the nose, particularly at the high lift obtained by trailing-edge flap blowing.

The figures showing the variation of lift coefficient with incidence and blowing coefficient as 'carpets' (Figs. 14 to 17) show clearly the improvement in lift coefficient attainable by blowing at trailing-edge flaps. This is accompanied by an increase in lift-curve slope from approximately 4·3/radian without blowing, at trailing-edge flap settings from 20° to 60°, to approximately 6·4/radian for trailing-edge flap angles of 20° and 40°, and 5·7/radian with trailing-edge flap at 60°, at the maximum blowing momentum used. With undeflected trailing-edge flaps the lift-curve slope is 6·05/radian without blowing, and 6·5/radian with a momentum coefficient of 0·019 at the trailing-edge flap.

4.2.2. *Pitching moment.* The curves in which coefficients of pitching moment are plotted against those of lift (Figs. 18 to 22) show that the effects of blowing on the stability of the isolated two-dimensional section are progressive, without any marked changes of behaviour. With flaps undeflected the wing has neutral stability about the quarter-chord point, and this is little affected by blowing. Deflection of the unblown trailing-edge flap causes a progressively increasing instability; at the smaller flap deflections blowing tends to reduce this instability, but with flaps at 60° the lower blowing quantities give a further loss of stability, a value for dC_m/dC_L of +0·3 being obtained near the stall with a blowing momentum coefficient of 0·06.

4.2.3. *Drag.* Coefficients of drag derived from the wake rake measurements are plotted against incidence in Figs. 23 to 26. Variation of drag with incidence is generally of parabolic form, exceptions being the sharp rise in drag at low incidence with undeflected trailing-edge flaps and drooped nose, where there is evidently a separation from the leading-edge lower surface, and the fall in drag at high incidence with trailing-edge flaps at 60° and with blowing at the leading-edge flap knee. At constant incidence, approximately 70 per cent of the momentum of the jet appears as a reduction of drag; the remainder is probably accounted for by losses in the blowing nozzles and by increased aerodynamic drag at the higher lift attained with increase of blowing momentum. If the nozzle losses are assumed to be fairly small, the aerodynamic drag is given by the sum of the measured drag and blowing momentum coefficients. $(C_D + C'_{\mu R})$ is plotted against lift coefficient in Fig. 27. It is possible on this figure to draw lines which are approximately minimum envelopes of the individual curves, taking the two leading-edge flap angles separately. Most of the individual curves tend towards tangency with these curves, although where the blowing momentum is either too low to prevent separation from the trailing-edge flap or well above the

*Suction was applied over a narrow strip of the tunnel roof and floor turntables, immediately adjacent to the wing upper surface[2].

attachment value the curve is well above the optimum. The envelope curves show approximately the minimum aerodynamic drag which can be obtained with the optimum choice of flap setting, incidence and blowing momentum for a given lift coefficient.

4.2.4. *Boundary-layer measurements.* To illustrate the boundary-layer parameters measured, Figs. 28 to 30 show, for trailing-edge flap angles of 20° and 40°, the increase in boundary-layer momentum thickness measured between the rake forward of the blowing slot and that near the flap trailing-edge. Also shown for a trailing-edge flap angle of 20° is a curve of the instantaneous theoretical change in momentum thickness resulting from injecting the momentum given by $C'_{\mu R}$. The slope of the measured momentum-thickness curves is similar, indicating that the change in momentum thickness introduced at the blowing slot is largely realised at the trailing edge.

Fig. 31 compares the development of the boundary layer ahead of the blowing slot, as calculated by Head's method[7], and as measured by the fixed rake and boundary-layer traverses. The calculations took as their starting conditions the measured boundary-layer values at $x/c = 0{\cdot}42$, and Fig. 31 shows reasonable agreement between quantities measured by the traverse, and those measured by the fixed rake.

4.3. *Comparisons with Inviscid Theory.*

It is possible, using a surface singularity method[8], to calculate the flow around the wing section in the presence of the wind-tunnel walls. The results of these calculations can be compared directly with the measured values, without correction for blockage or constraint, (provided the flow remains attached) since these corrections are made to obtain the equivalent 'unbounded stream' values. Such a comparison is shown in Fig. 32 for the case of the nose flap at 0° and the trailing-edge flap at 20°. As might be expected, the blowing momentum required to achieve the inviscid lift increases with incidence. Pressure distributions corresponding to the blowing coefficients required for the inviscid lift have been interpolated from the measured values, and Fig. 33 shows a typical comparison between the predictions of the inviscid theory and the experimental results.

A similar set of calculations have been made for the configuration with the nose flap deflected 30° and the trailing-edge flap deflected 60°. Fig. 34 compares the results from the inviscid theory with experimental results interpolated, as before, at the blowing coefficient at which the inviscid lift was achieved. Figs. 33 and 34 are similar in that there is quite close agreement between the theory and the experiment; in both cases the measured pressure coefficients on the upper surface tend to be lower than predicted over the front of the aerofoil, and higher at the rear. It is probable that this is due to the change in boundary-layer displacement thickness from a positive value over the front of the aerofoil to a negative value aft of the blowing slot.

Since fewer experimental results were obtained for a trailing-edge flap deflection of 40°, both with and without nose deflection, the extensive theoretical calculations for the wing with wall effect (involving a separate calculation at each angle of incidence of the flow around two infinite cascades of aerofoils) could not be justified. Instead, values of the lift in the presence of the walls were deduced from the free air values. Fig. 35 compares the free air lift coefficients and the lifts predicted in the presence of the walls, for the two configurations for which the full calculations were made. The ratio of the lift in wall effect to that in free air is shown in the upper figure of Fig. 36. Interpolation to a trailing-edge flap deflection of 40° was aided by the results calculated by de Jager and van der Vooren[9] for a thin wing with a trailing-edge flap, at zero incidence*. Their results for the appropriate flap/chord ratio and tunnel height : chord ratio are shown in the lower figure of Fig. 36, together with two values from the upper figure. The thick-wing results are approximately 1·007 times the thin-wing values. Hence a tunnel wall-effect factor can be established at zero incidence for a flap deflection of 40°, and a series of values interpolated through the incidence range.

When the assumed values at a flap deflection of 40° are compared with the experimental measurements, it is found that, within the experimental scatter, the momentum coefficient to achieve the inviscid lift is

*The effect of leading-edge flap deflection on lift at a given incidence and trailing-edge flap deflection is small, and it was considered that this would not alter the tunnel wall effect on lift.

independent of the nose deflection. Fig. 37 summarises the values of the momentum coefficient to achieve the inviscid lift. Also shown is a line which represents the minimum momentum coefficient to achieve the inviscid lift by variation of trailing-edge flap deflection and angle of incidence.

Finally the wake drag corresponding to the inviscid lift has been interpolated from Figs. 24 to 26, and the sum of the wake drag and blowing momentum evaluated. These values are compared in Fig. 38 with the two optimum lines derived in Fig. 27. The results for zero nose deflection lie slightly above the optimum line, whilst those for 30° nose deflection lie close to the optimum line. There is, therefore, some grounds for considering that the optimum drag performance occurs when the inviscid lift is achieved.

5. *Conclusions.*

These experiments have shown, for a range of trailing-edge flap deflections, the effectiveness of boundary-layer control by blowing for increasing the lift capability of a wing section. The increases of stalling incidence, and maximum lift, due to the deflection of a nose flap, possibly with boundary-layer control by blowing, have also been demonstrated. The associated pitching moment and wake drag values have been measured.

Comparisons with the predictions of an inviscid theory show that very similar pressure distributions can be achieved at values of the blowing momentum which vary with angle of incidence and flap deflection. There is some evidence to suggest that a minimum value of the term (wake drag + blowing momentum) occurs when the inviscid lift is achieved.

Acknowledgement.

The wind-tunnel department of the British Aircraft Corporation at Weybridge provided the staff for these tests, and performed the initial reduction of the results.

LIST OF SYMBOLS

a	Fraction of chord from leading edge over which the loading is uniform at the ideal angle of attack
c	Wing chord
C_D	Drag coefficient
C_L	Lift coefficient
$C_{L_{opt}}$	Section design lift coefficient
$C_{m\frac{1}{4}}$	Pitching-moment coefficient about quarter-chord point
C_p	Pressure coefficient
C'_μ	Sectional blowing momentum rate coefficient $= \frac{m_J V_J}{\frac{1}{2}\rho_0 V_0^2 S}$
m_s, m_j	Suction and blowing mass-flow rates
P	Absolute pressure
R	Reynolds number
S	Wing area
t	Wing maximum thickness
V_J	Slot blowing velocity
V_0	Tunnel free-stream velocity
x	Distance along chord line
α	Angle of incidence
δ^*	Displacement thickness of boundary layer on tunnel roof or floor, at position of model, tunnel empty
η	Angle of deflection of flaps
θ	Momentum thickness of boundary layer on wing surface
ρ_0	Tunnel free-stream density

Suffices

A	Atmospheric conditions
B	Blowing nozzle reference conditions
N	Nose flap
R	Rear flap
S	Jet stagnation conditions

REFERENCES

No.	*Author(s)*	*Title, etc.*
1	J. Williams and S. F. J. Butler	Aerodynamic aspects of boundary-layer control for high lift at low speeds. *J. R. Ae. Soc.*, Vol. 67, pp 201–223. R.A.E. Technical Note Aero 2858, A.R.C. 24535, AGARD Report 414 (1966).
2	D. N. Foster and J. A. Lawford	Experimental attempts to obtain uniform loading over two-dimensional high-lift wings. R.A.E. Technical Report 68283 A.R.C. 31 098 (1968).
3	D. N. Foster and J. A. Lawford	Initial low-speed tunnel tests on the effect of pressure ratio on blowing over trailing-edge flaps. R.A.E. Unpublished paper (1968).
4	D. S. Woodward	On the errors induced at tunnel reference pressure tappings by high-lift models. R.A.E. Technical Report 66 049 (1966).
5	H. C. Garner, E. W. E. Rogers, W. E. A. Acum and E. C. Maskell	Subsonic wind tunnel wall corrections. AGARDOGRAPH 109 (1966).
6	B. Melvill Jones	Measurement of profile drag by the pitot-traverse method. A.R.C. R. & M. 1688 (1936).
7	M. R. Head	Entrainment in the turbulent boundary layer. A.R.C. R. & M. 3152 (1960).
8	D. N. Foster	Note on methods of calculating the pressure distribution over the surface of twodimensional cambered wings. R.A.E. Technical Report 67 095, A.R.C. 29 419 (1967).
9	E. M. de Jager and A. I. v. d. Vooren	Tunnel wall corrections for a wing-flap system between two parallel walls. N.L.R. Report W.7 (1961).

TABLE 1

Details of Model.

Aerofoil chord = 4 ft (1·22 m)

Leading-edge flap chord = 0·125 wing chord

Trailing-edge flap chord = 0·250 wing chord

Both flaps hinged on lower surface

Aerofoil co-ordinates.

x/c	z/c	
	Upper surface	Lower surface
0	0	0
0·005	0·01146	−0·01000
0·0075	0·01415	−0·01201
0·0125	0·01845	−0·01531
0·025	0·02840	−0·02094
0·05	0·03754	−0·02822
0·075	0·04580	−0·03328
0·10	0·05243	−0·03713
0·15	0·06260	−0·04272
0·20	0·06987	−0·04643
0·25	0·07496	−0·04878
0·30	0·07820	−0·05004
0·35	0·07968	−0·05030
0·40	0·07927	−0·04951
0·45	0·07656	−0·04746
0·50	0·07226	−0·04454
0·55	0·06680	−0·04100
0·60	0·06049	−0·03703
0·65	0·05353	−0·03273
0·70	0·04613	−0·02823
0·75	0·03845	−0·02361
0·80	0·03067	−0·01899
0·85	0·02288	−0·01436
0·90	0·01514	−0·00970
0·95	0·00748	−0·00494
1·00	0	0

TABLE 2

Details of Tests.

η_N°	η_R°	$C'_{\mu N}$	$C'_{\mu R}$	Remarks
0	0	0	0	0·025 in faired step (all other tests, 0·060 in step)
0	0	0	0	slot faired
0	0	0	0*	slot open
0	0	0	0	slot faired. Reynolds number range from $1{\cdot}29 \times 10^6$ to $5{\cdot}87 \times 10^6$
0	0	0	0·019*	
30	0	0	0*	slot faired
0	20	0	0 0·008 0·013 0·017* 0·026* 0·036 0·048*	
0	40	0	0 0·018* 0·037* 0·050* 0·060	
30	40	0	0 0·022* 0·038* 0·053* 0·066	
30	40	0·013 0·022	0·038 0·038	
30	60	0	0 0·060* 0·078 0·091* 0·096 0·103 0·113*	
30	60	0·014 0·025	0·078 0·089* 0·078 0·089*	

*Denotes drag measured by wake-survey technique.

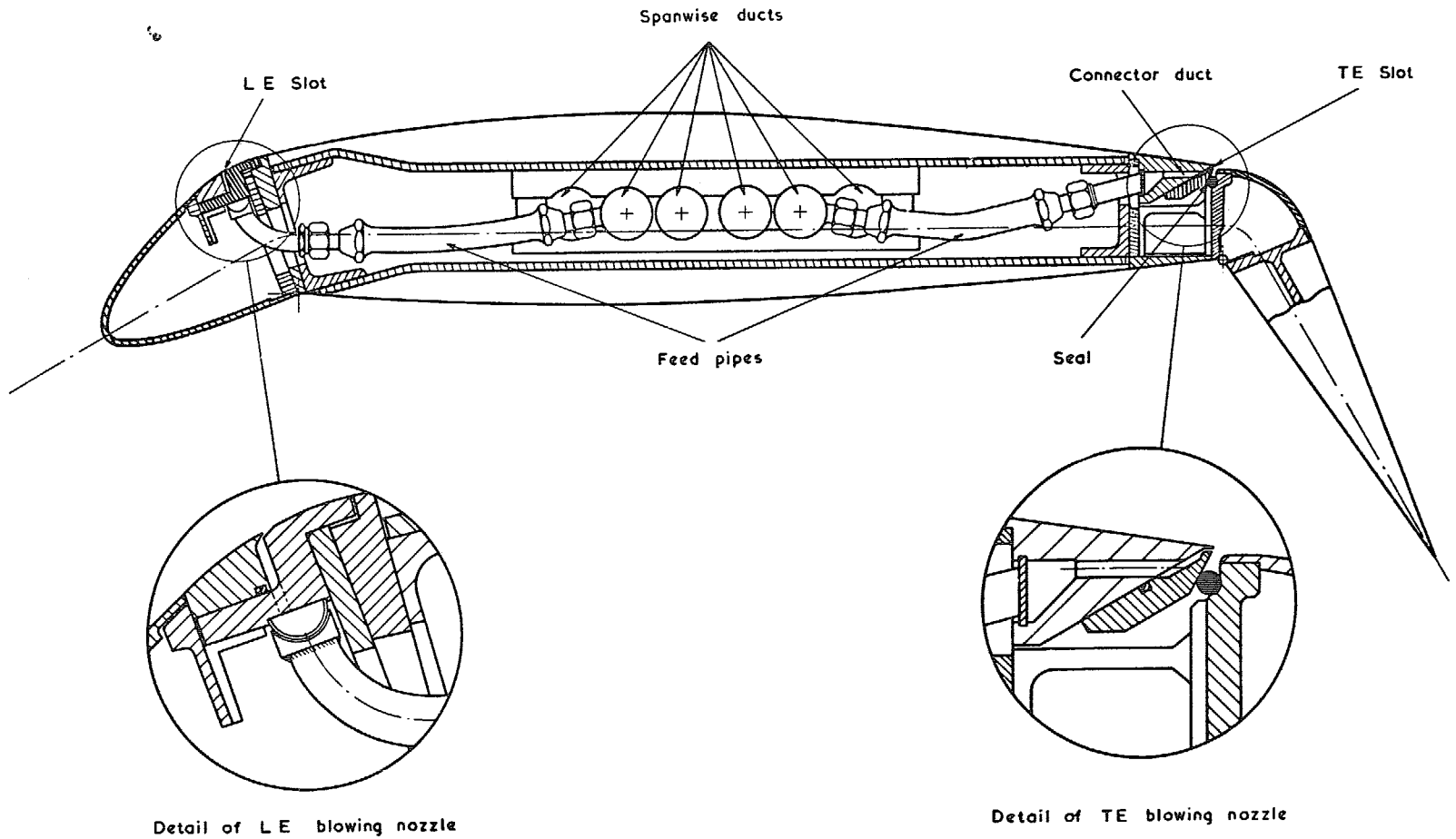

FIG. 1. Typical section of the model.

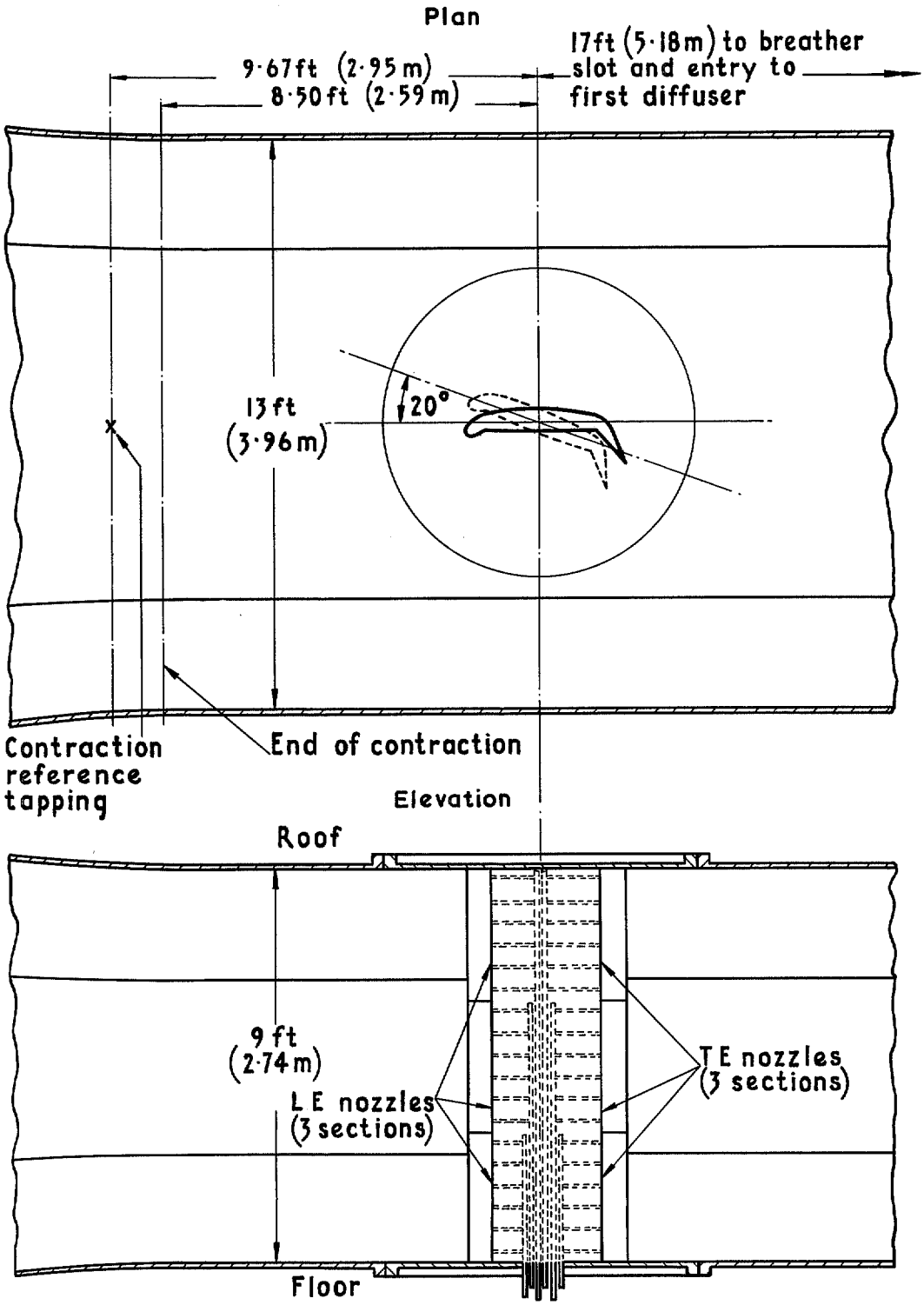

FIG. 2. Mounting of model in wind tunnel (diagrammatic); wall suction details omitted for clarity.

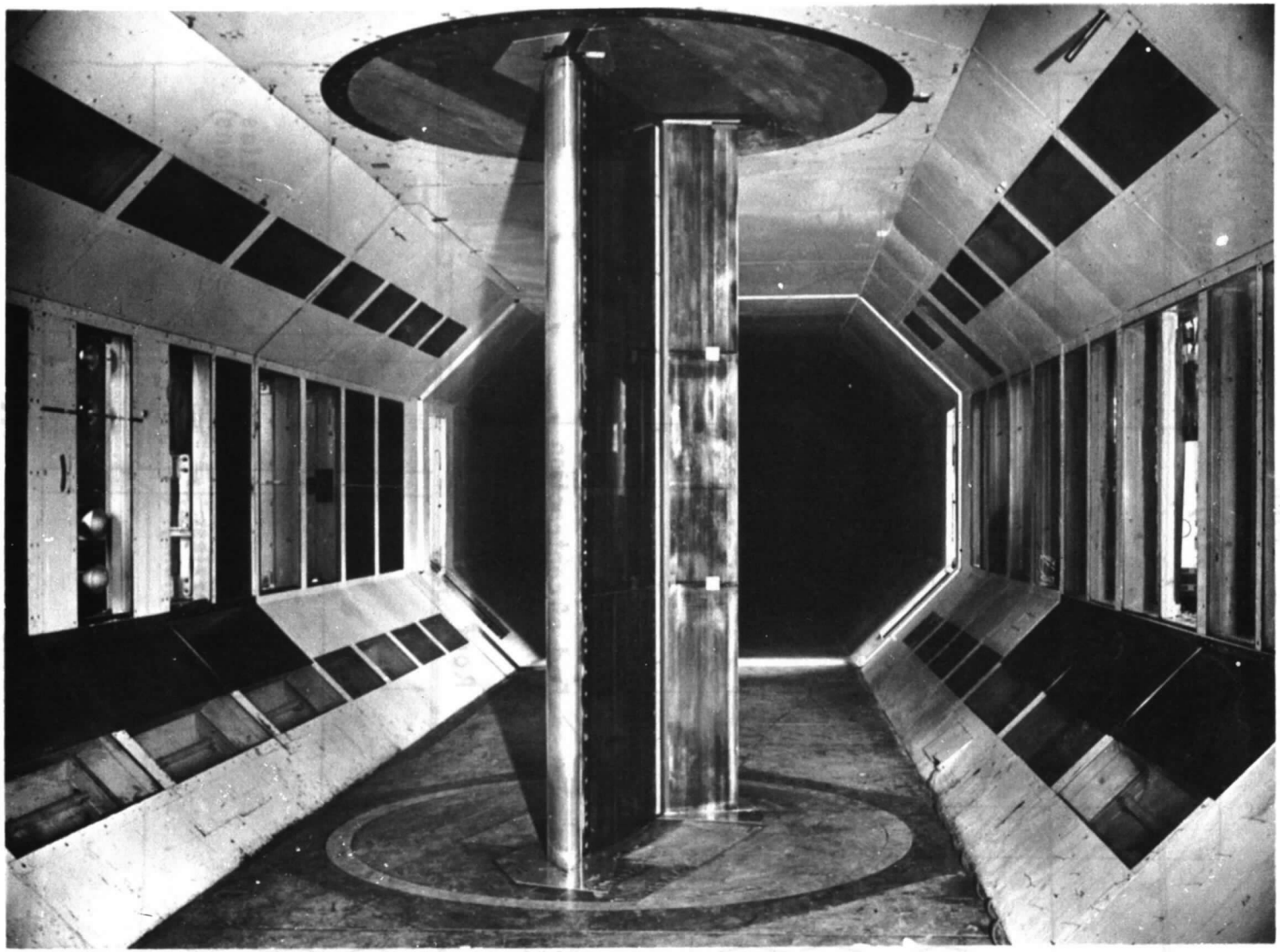

FIG. 3. Model in wind tunnel.

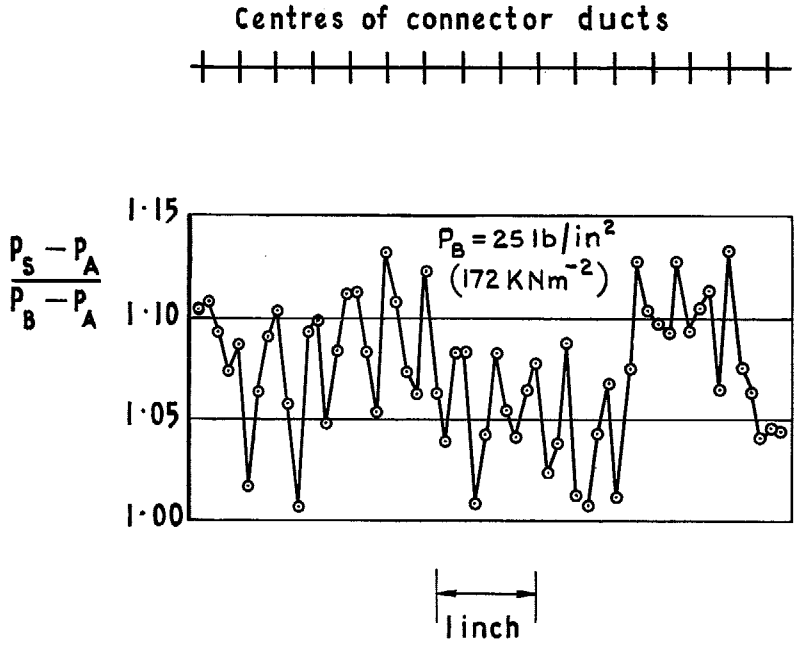

FIG. 4. Typical stagnation-pressure distributions along slot.

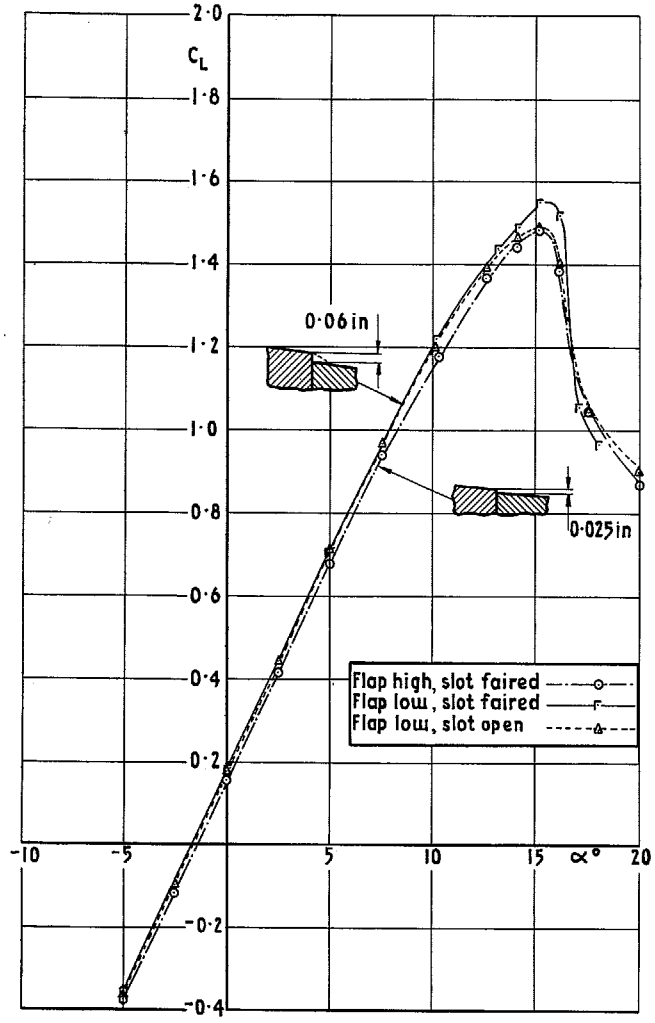

FIG. 5. Effect of rearward step at flap hinge. $\eta_N = 0°\ \eta_R = 0°$.

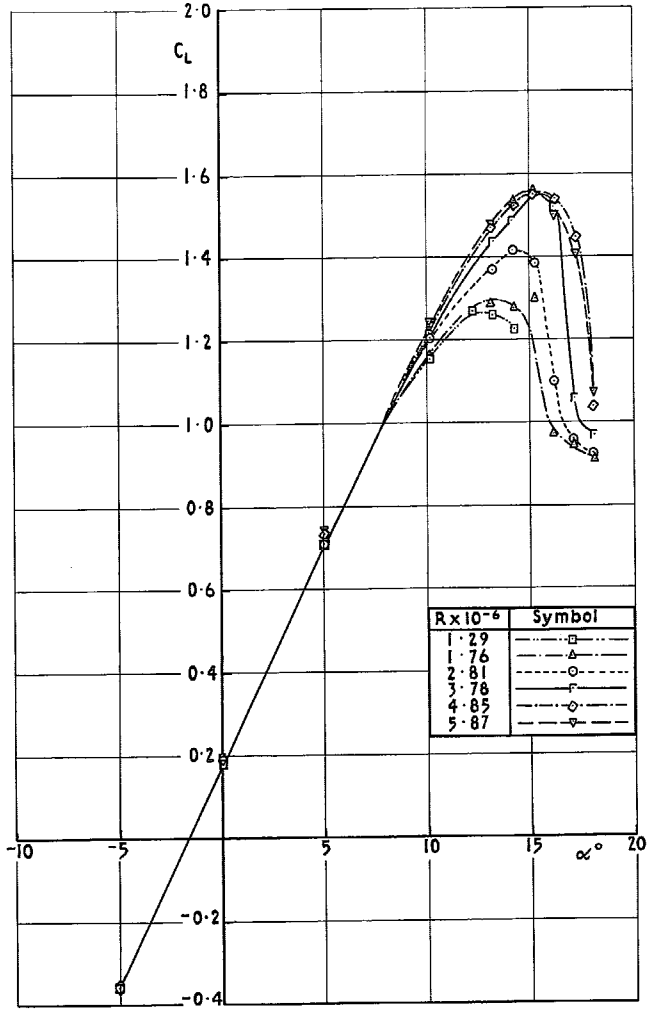

FIG. 6. Effect of Reynolds number on lift curve. $\eta_N = 0°$ $\eta_R = 0°$.

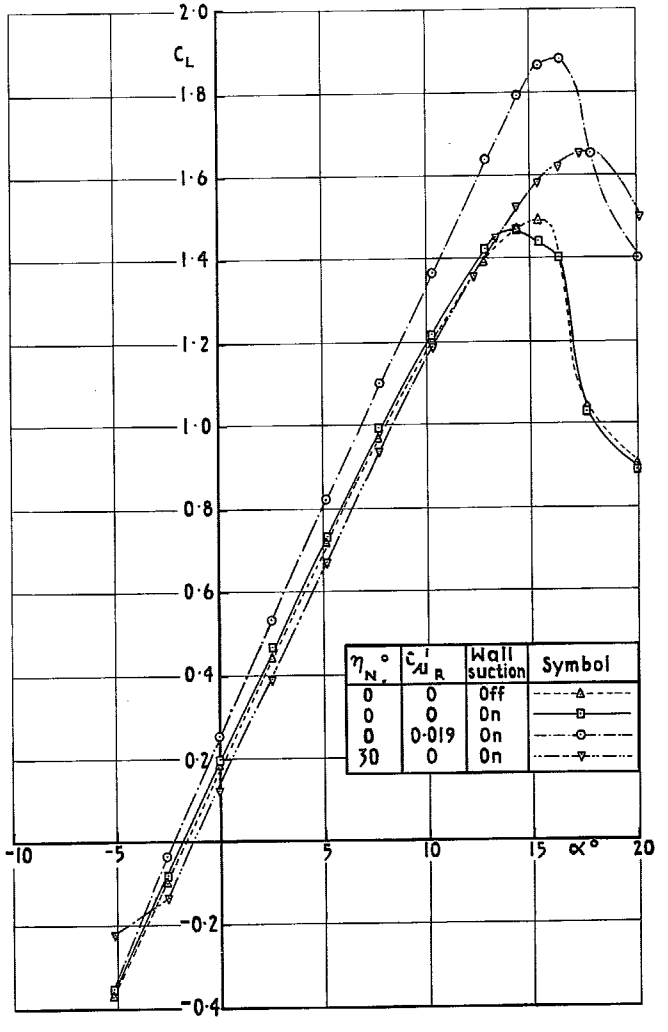

FIG. 7. Effect of nose deflection, wall suction and blowing on lift curve. $\eta_R = 0°$.

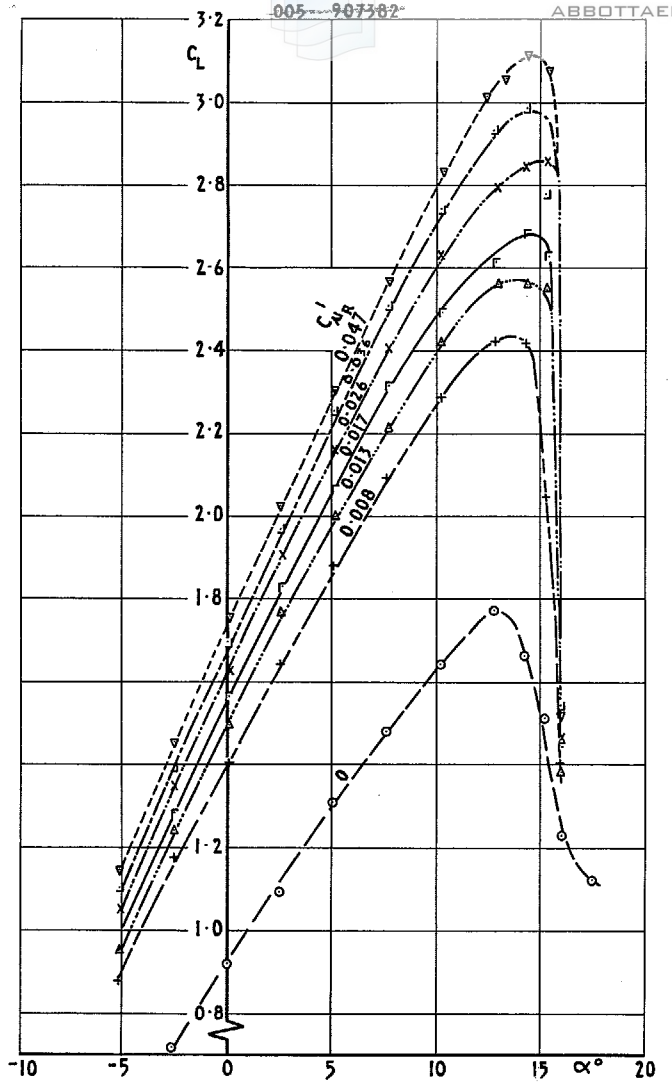

FIG. 8. Effect of blowing on lift curve.
$\eta_N = 0°, \eta_R = 20°, C'_{\mu_N} = 0$.

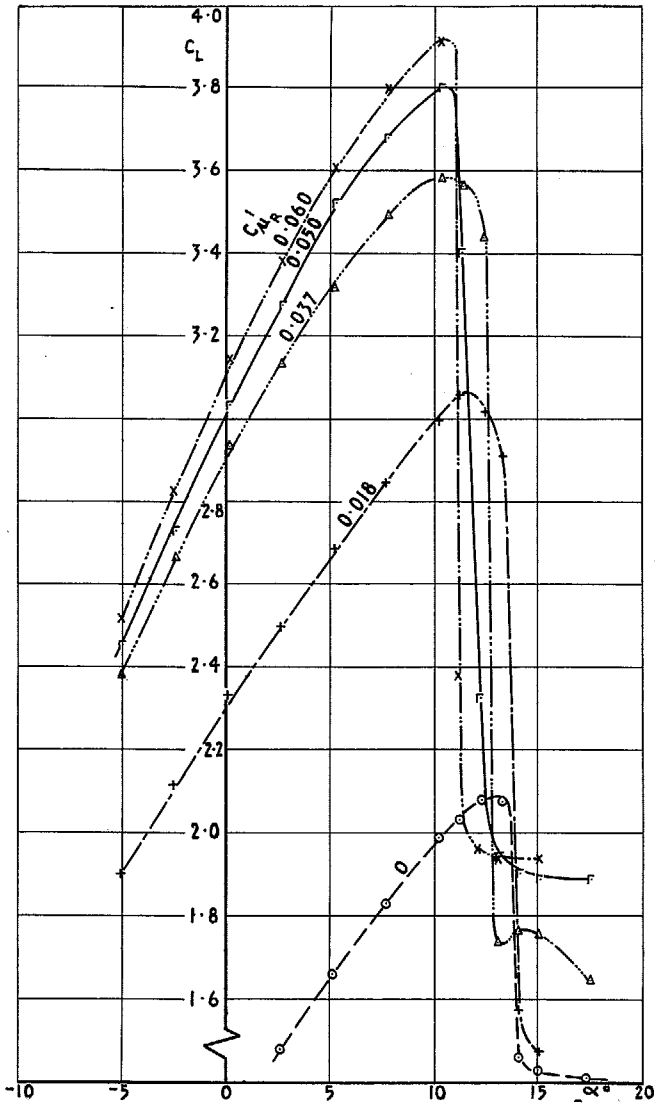

FIG. 9. Effect of blowing on lift curve.
$\eta_N = 0°, \eta_R = 40°, C'_{\mu_N} = 0$.

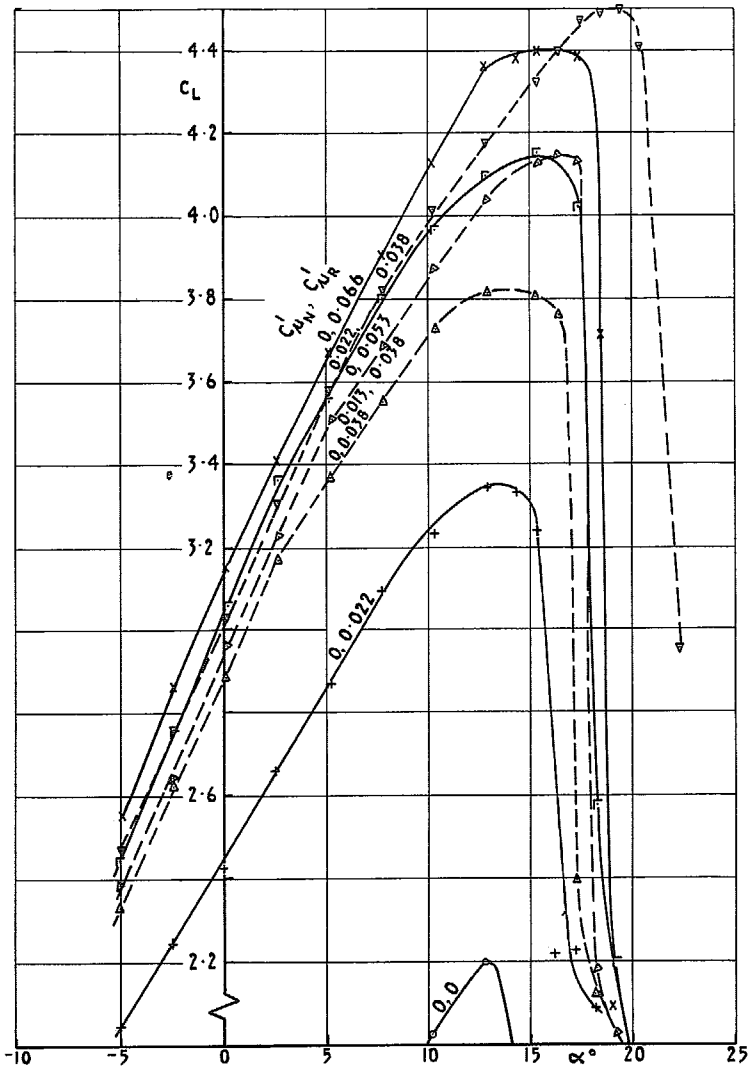

FIG. 10. Effect of blowing at nose flap on lift.
$\eta_N = 30°, \eta_R = 40°$.

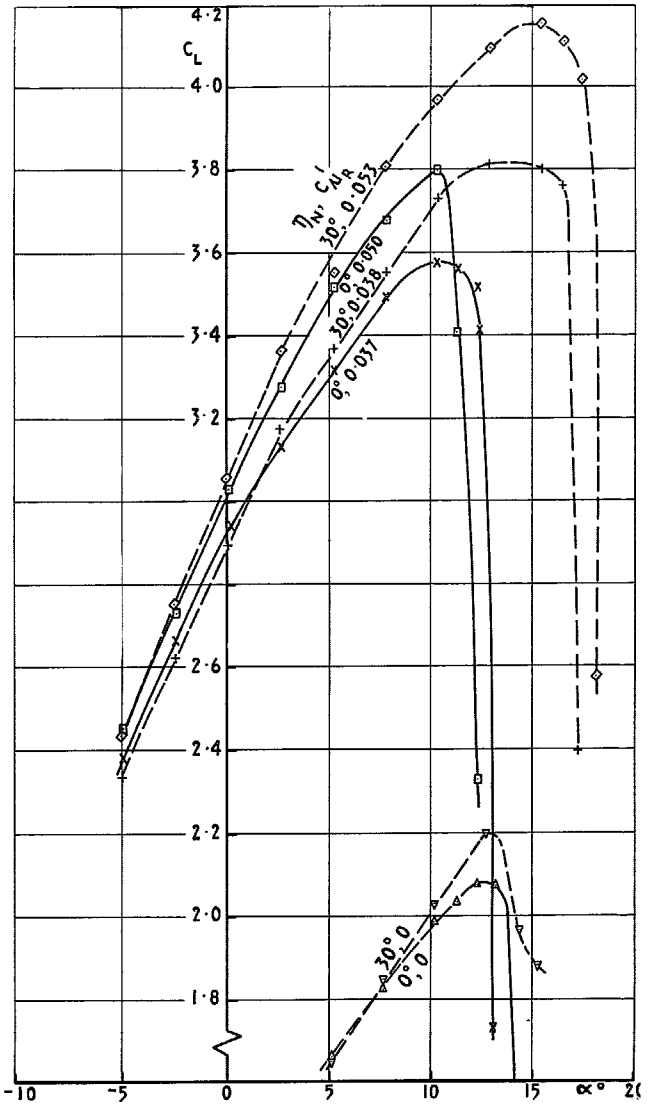

FIG. 11. Effect on deflection of nose flap on lift.
$\eta_R = 40°, C'_{\mu_N} = 0$.

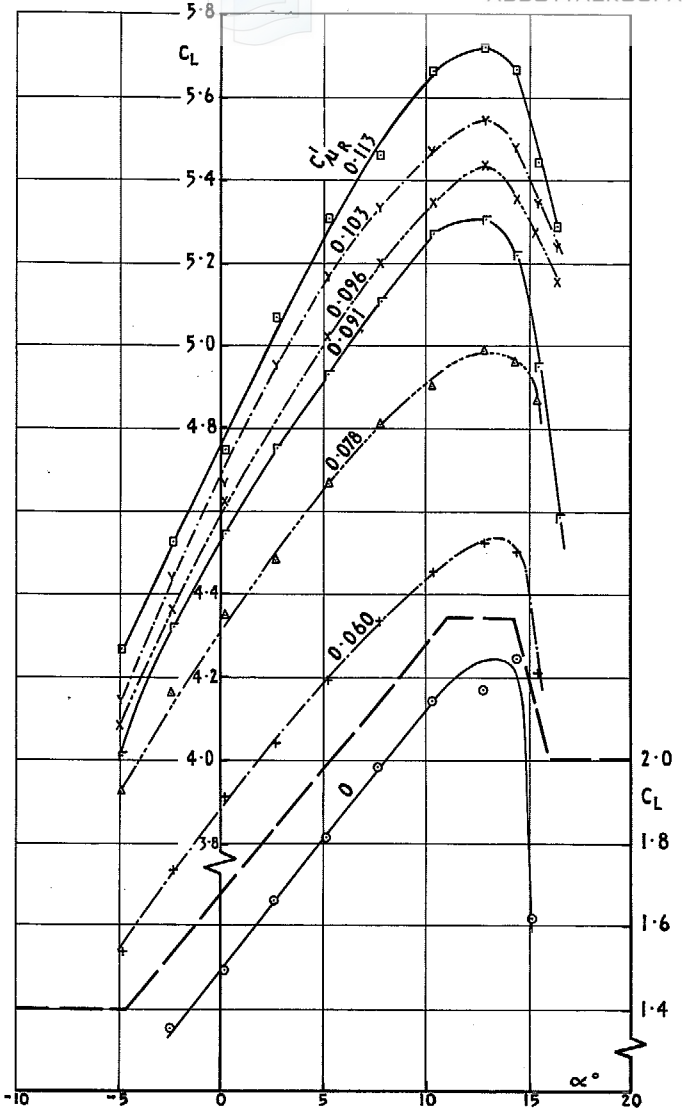

FIG. 12. Effect of blowing on lift curve.
$\eta_N = 30°, \eta_R = 60°, C'_{\mu_N} = 0$.

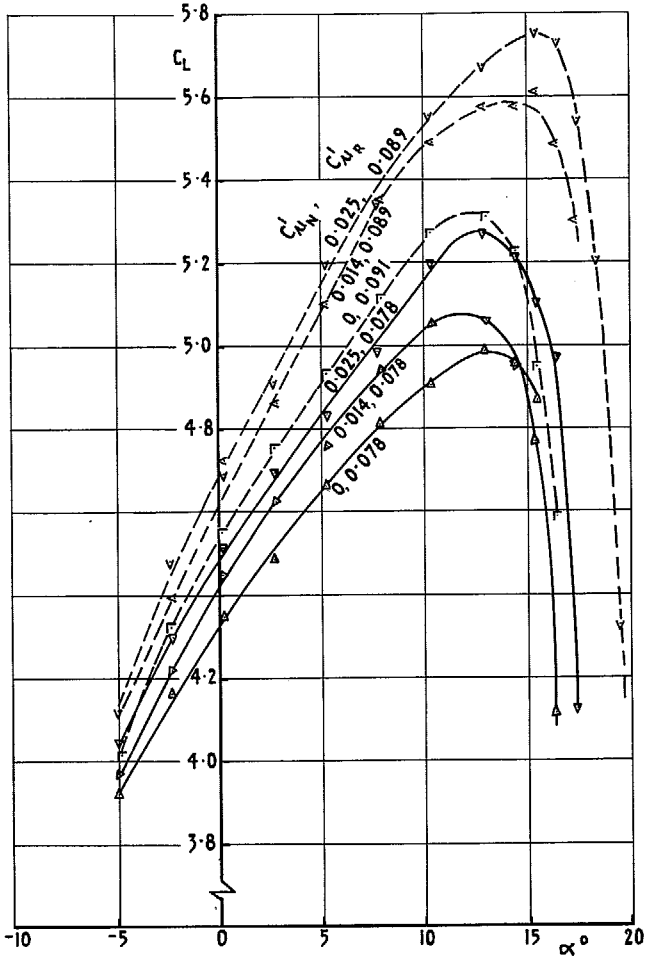

FIG. 13. Effect of blowing at nose flap on lift.
$\eta_N = 30°, \eta_R = 60°$.

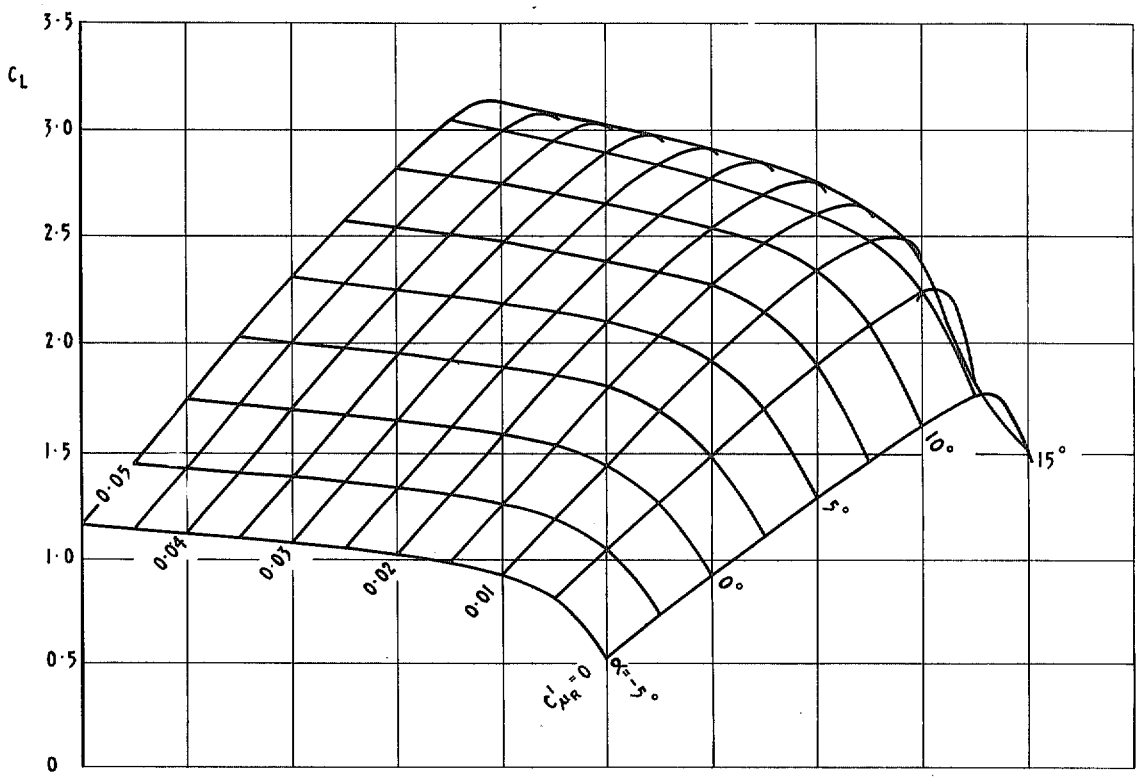

FIG. 14. Lift coefficient *vs.* incidence and T.E. blowing coefficient.
$\eta_N = 0°$, $\eta_R = 20°$, $C'_{\mu_N} = 0$.

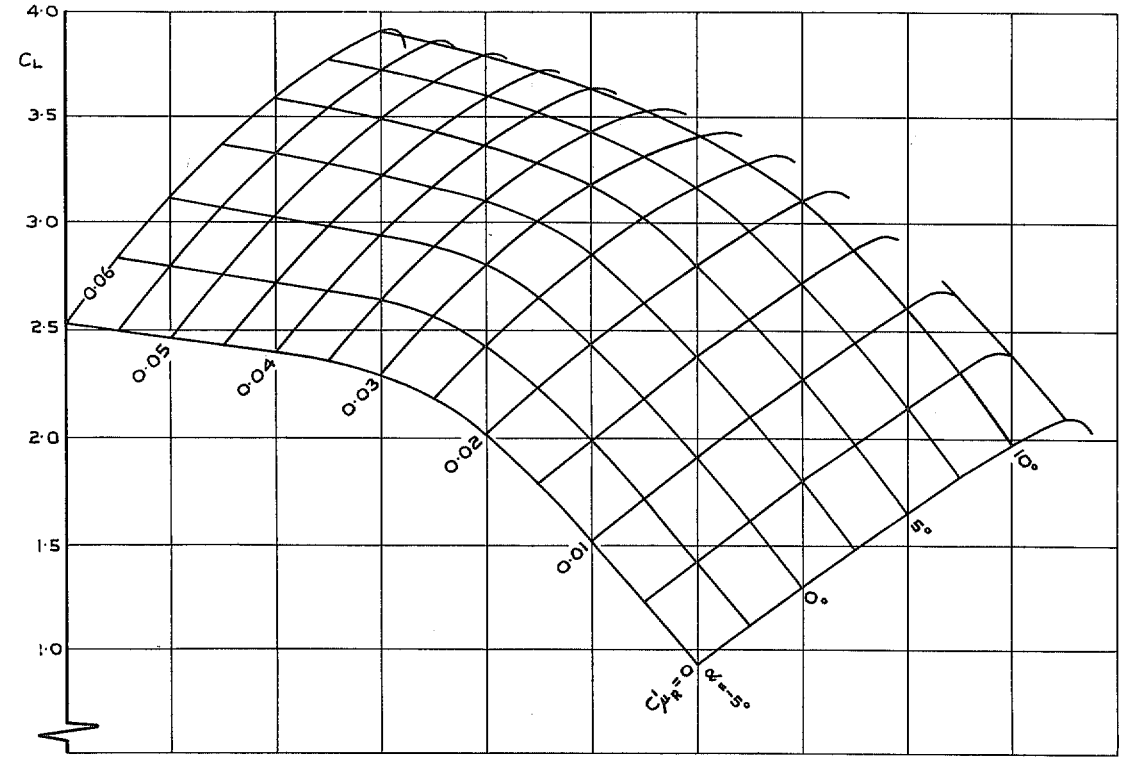

FIG. 15. Lift coefficient *vs.* incidence and T.E. blowing coefficient.
$\eta_N = 0°$, $\eta_R = 40°$, $C'_{\mu_N} = 0$.

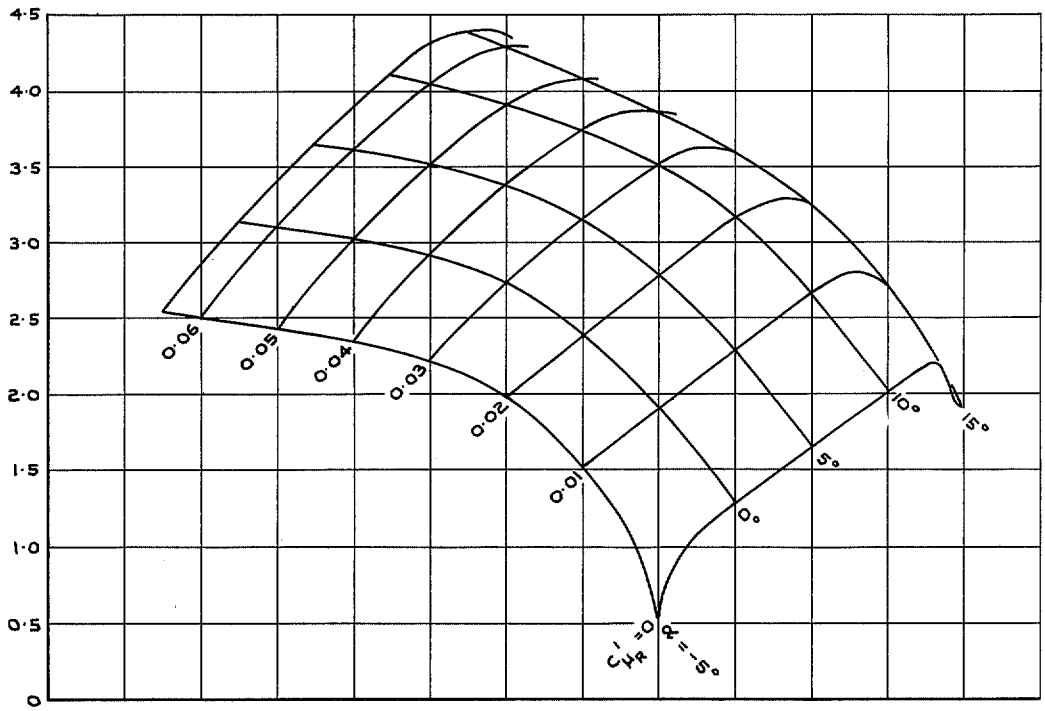

FIG. 16. Lift coefficient *vs.* incidence and T.E. blowing coefficient.
$\eta_N = 30°, \eta_R = 40°, C'_{\mu_N} = 0.$

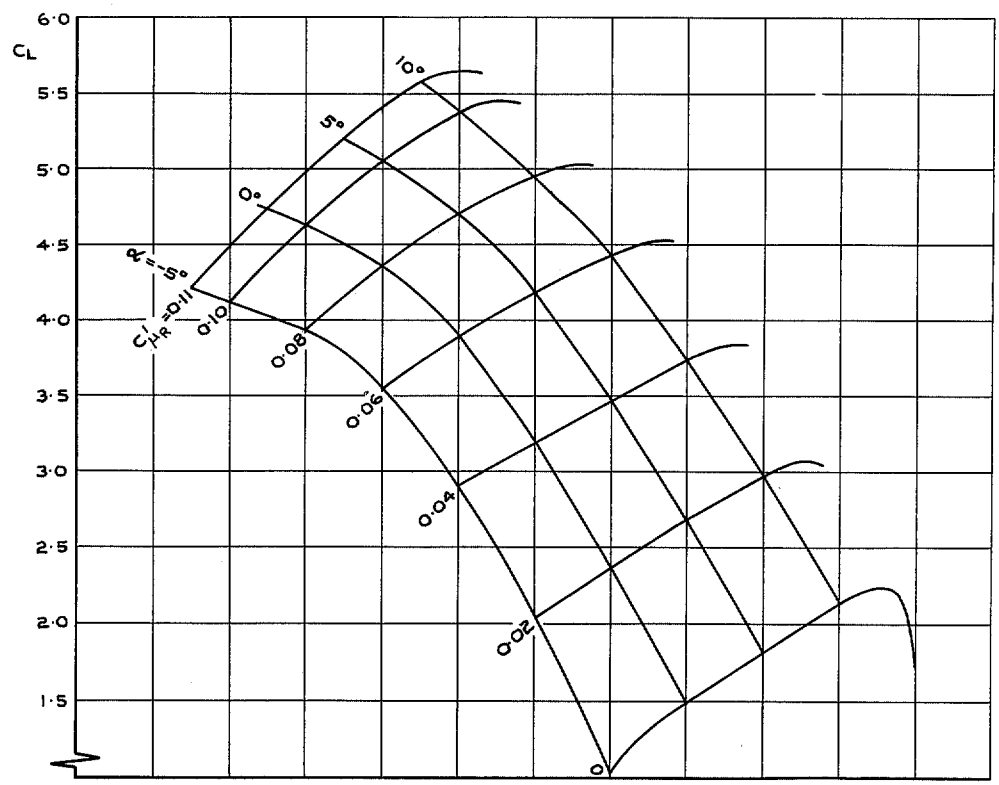

FIG. 17. Lift coefficient *vs.* incidence and T.E. blowing coefficient.
$\eta_N = 30°, \eta_R = 60°, C'_{\mu_N} = 0.$

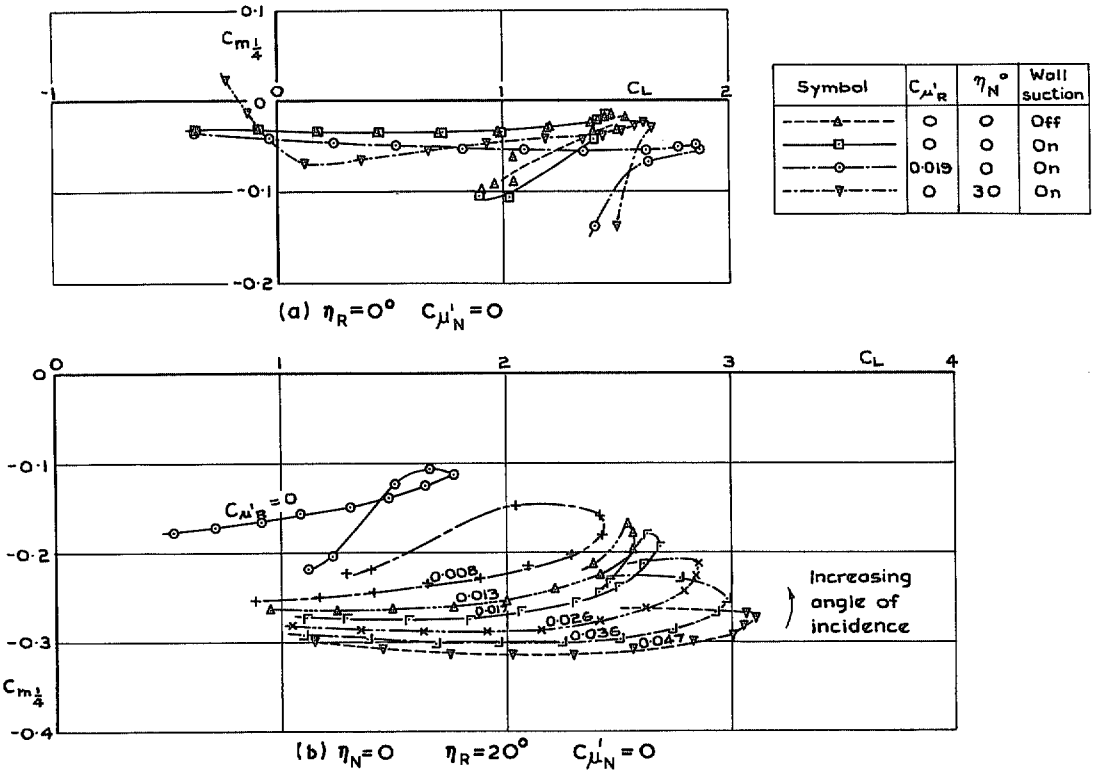

FIG. 18. Effect of flap deflection, wall suction and blowing on pitching moment.

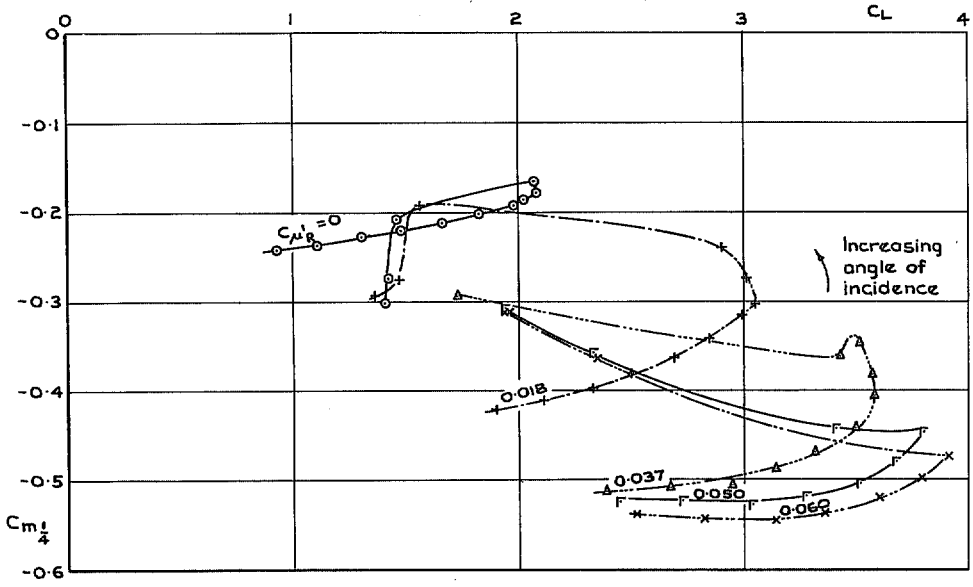

FIG. 19. Effect of blowing on pitching moment.
$\eta_N = 0°$, $\eta_R = 40°$, $C'_{\mu_N} = 0$.

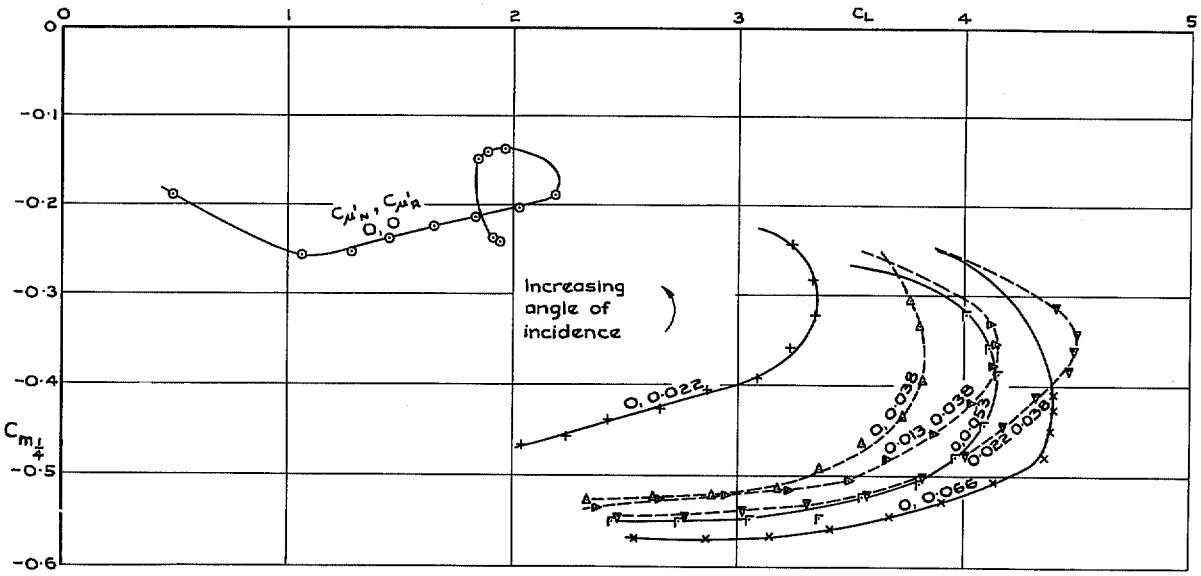

FIG. 20. Effect of blowing at nose flap on pitching moment.
$\eta_N = 30°, \eta_R = 40°$.

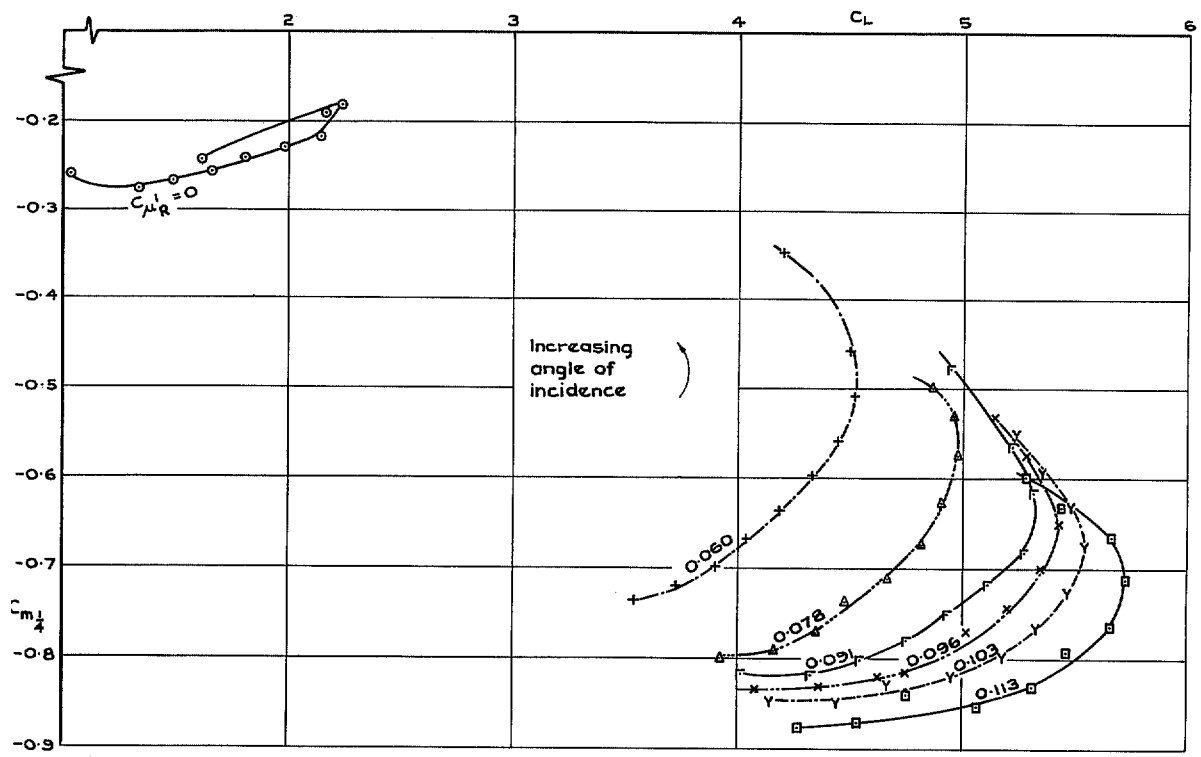

FIG. 21. Effect of blowing on pitching moment.
$\eta_N = 30°, \eta_R = 60°, C'_{\mu_N} = 0$.

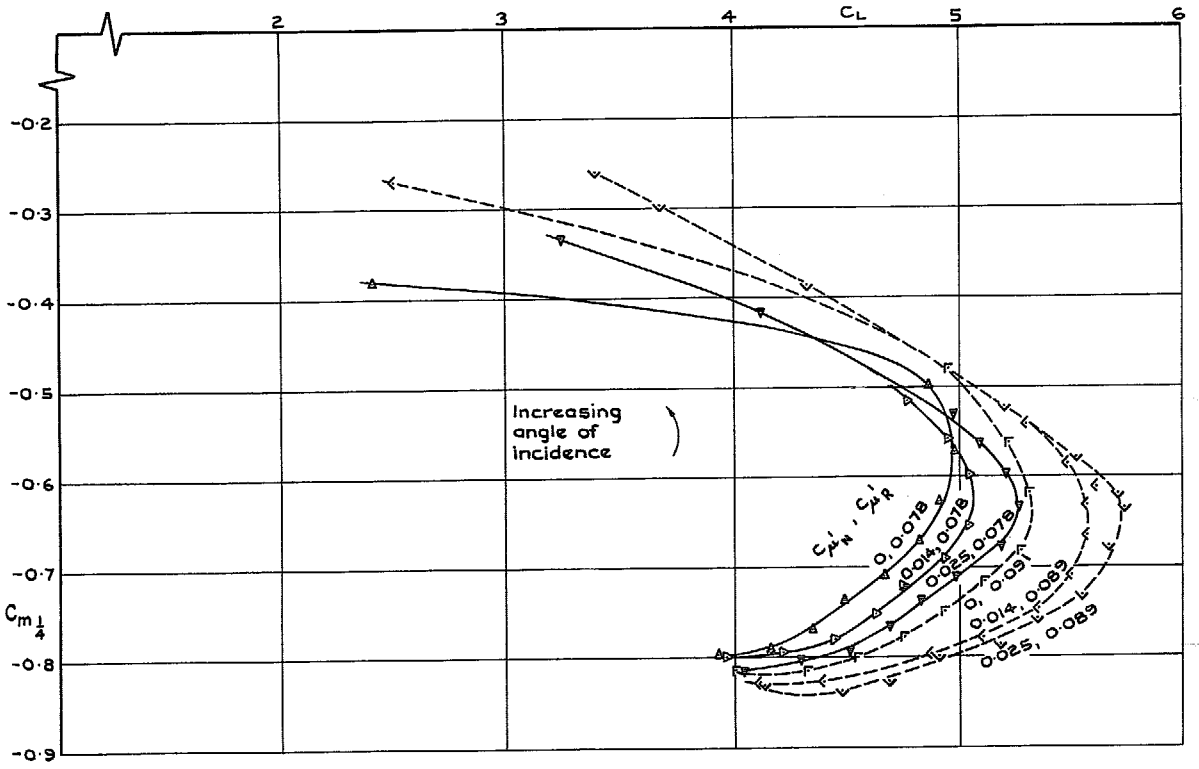

FIG. 22. Effect of blowing at nose flap on pitching moment.
$\eta_N = 30°$, $\eta_R = 60°$.

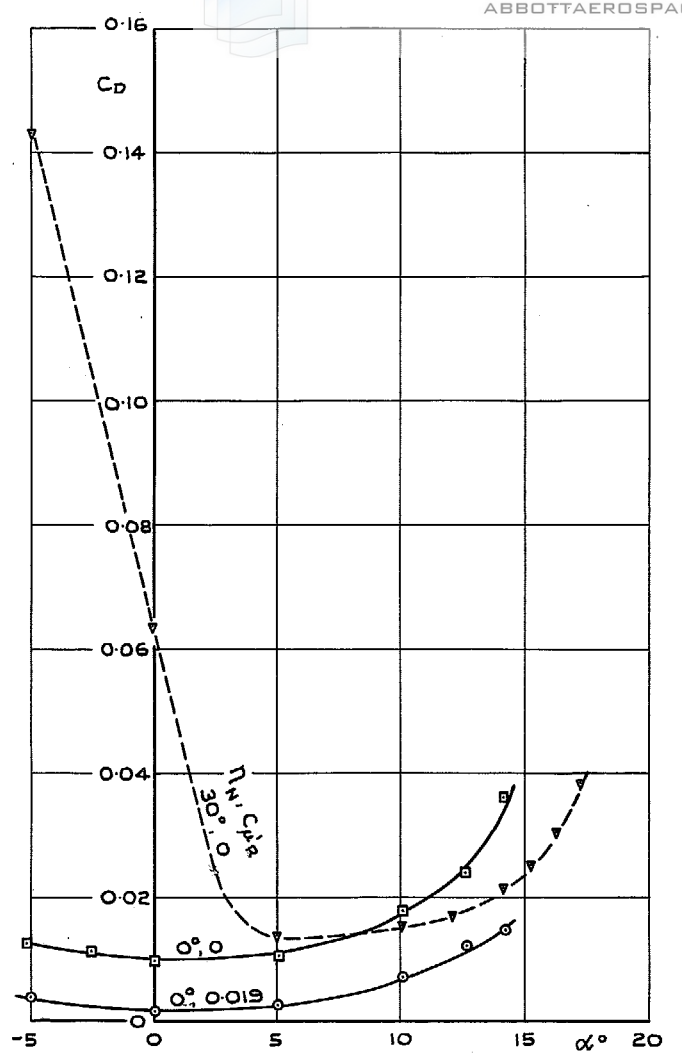

FIG. 23. Effect of nose deflection and blowing on wake drag.
$\eta_R = 0°$, $C'_{\mu N} = 0$.

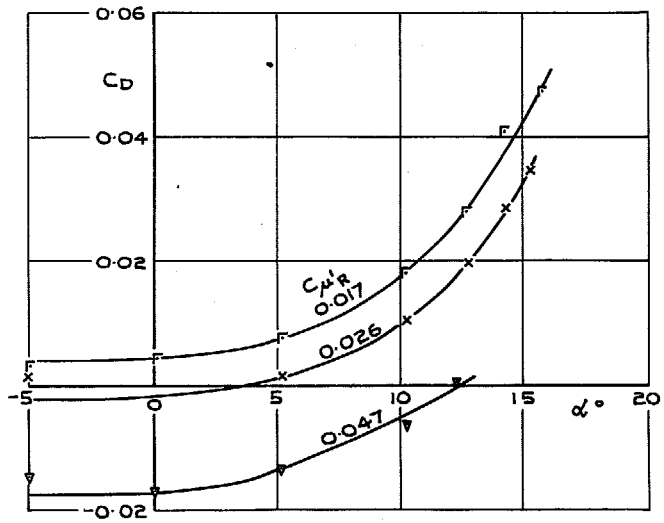

FIG. 24. Effect of blowing on wake drag.
$\eta_N = 0°$, $\eta_R = 20°$, $C'_{\mu N} = 0$.

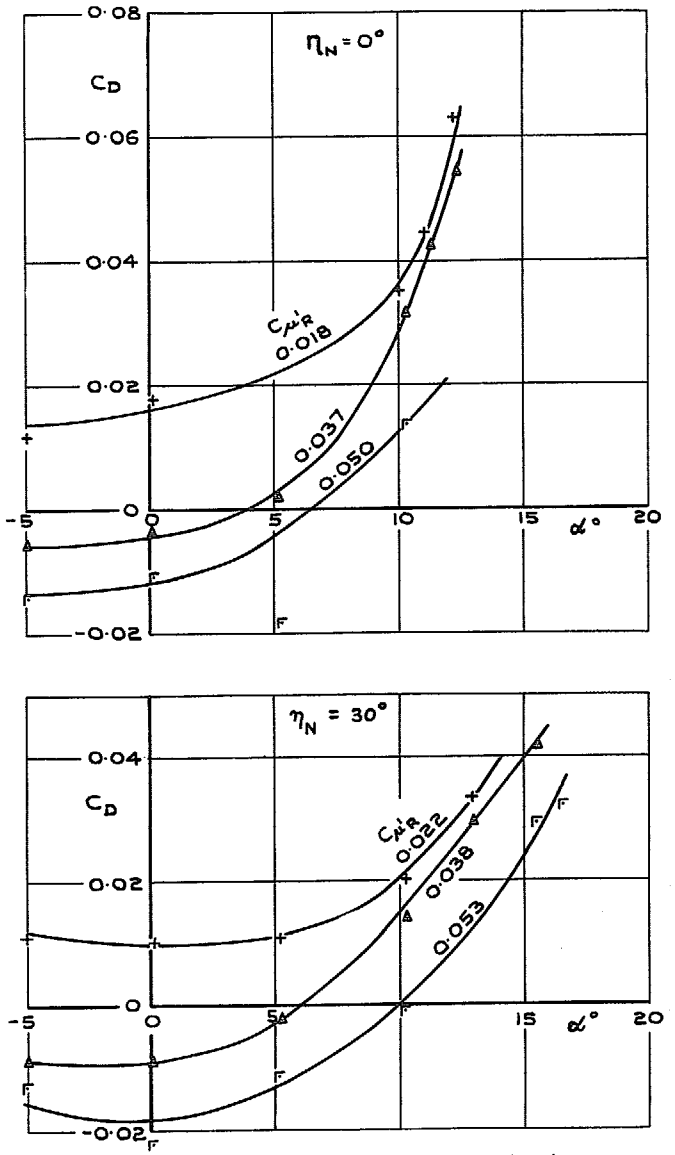

FIG. 25. Effect of nose deflection and blowing on wake drag.
$\eta_R = 40°$, $C'_{\mu_N} = 0$.

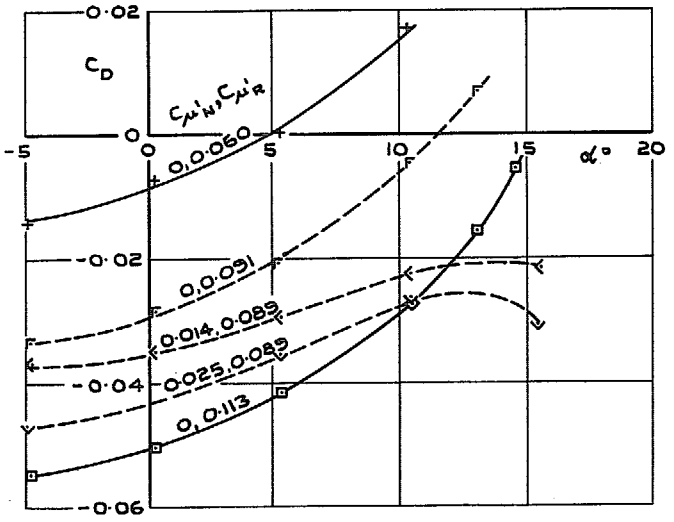

FIG. 26. Effect of blowing over nose and rear flap on wake drag.
$\eta_N = 30°$, $\eta_R = 60°$.

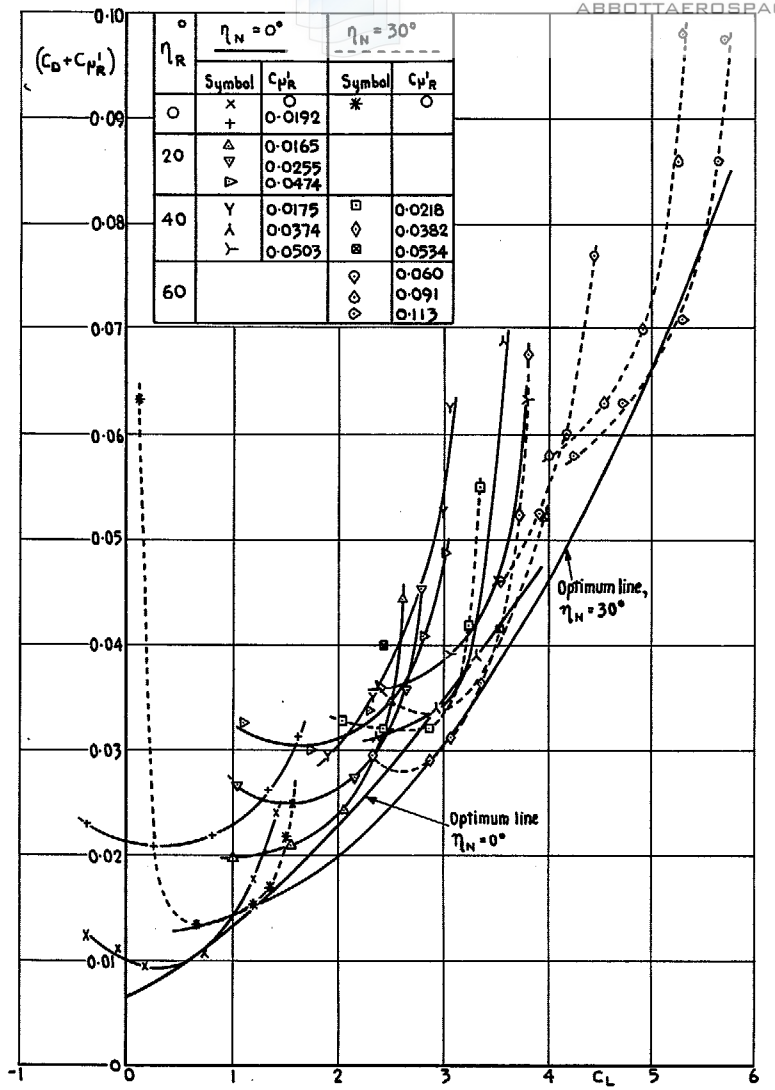

FIG. 27. Wake drag + blowing coefficient *vs.* lift coefficient.

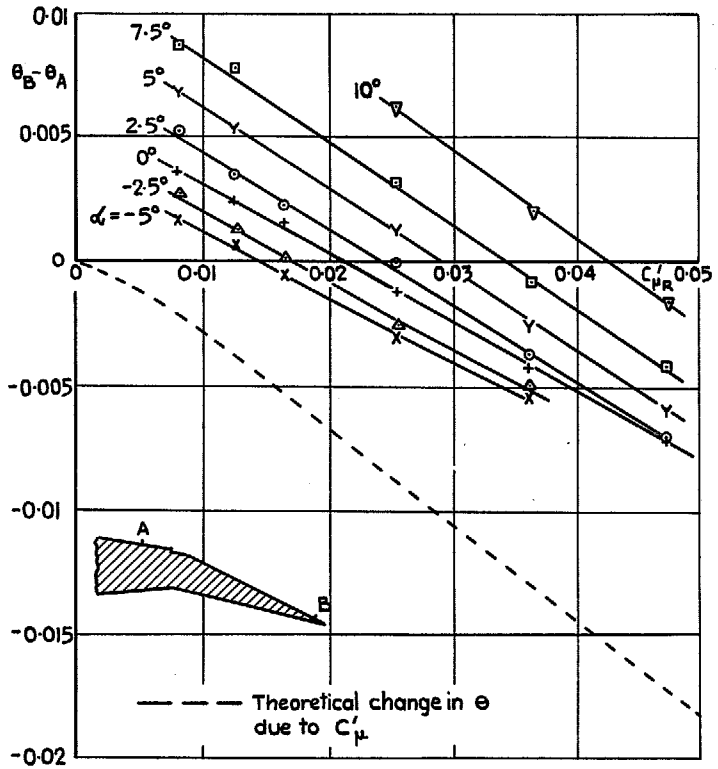

FIG. 28. Difference between momentum thicknesses forward of blowing slot and on the flap. $\eta_N = 0°$, $\eta_R = 20°$, $C'_{\mu N} = 0$.

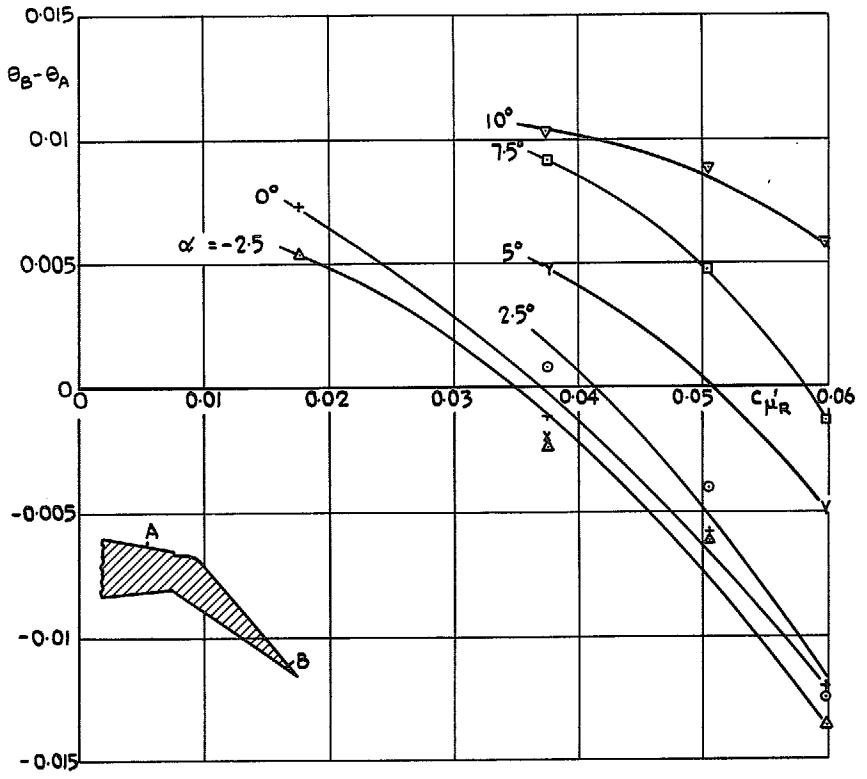

Position A is 0·04 c ahead of blowing slot
Position B is 0·02 c ahead of trailing-edge

FIG. 29. Difference between momentum thicknesses forward of the blowing slot and on the flap.
$\eta_N = 0°, \eta_R = 40°, C'_{\mu_N} = 0.$

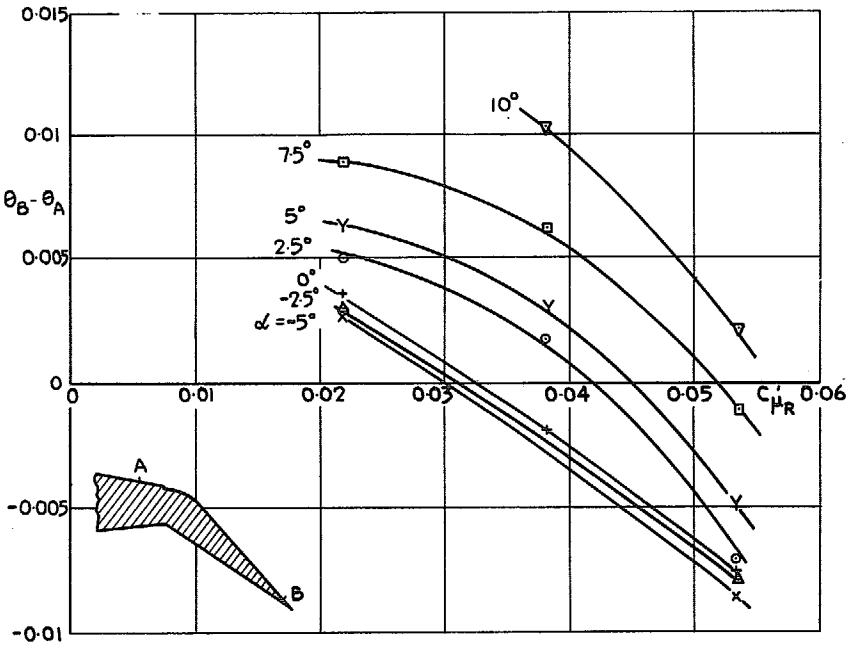

Position A is 0·04 c ahead of blowing slot
Position B is 0·02 c ahead of trailing-edge

FIG. 30. Difference between momentum thicknesses forward of the blowing slot and on the flap.
$\eta_N = 30°, \eta_R = 40°, C'_{\mu_N} = 0.$

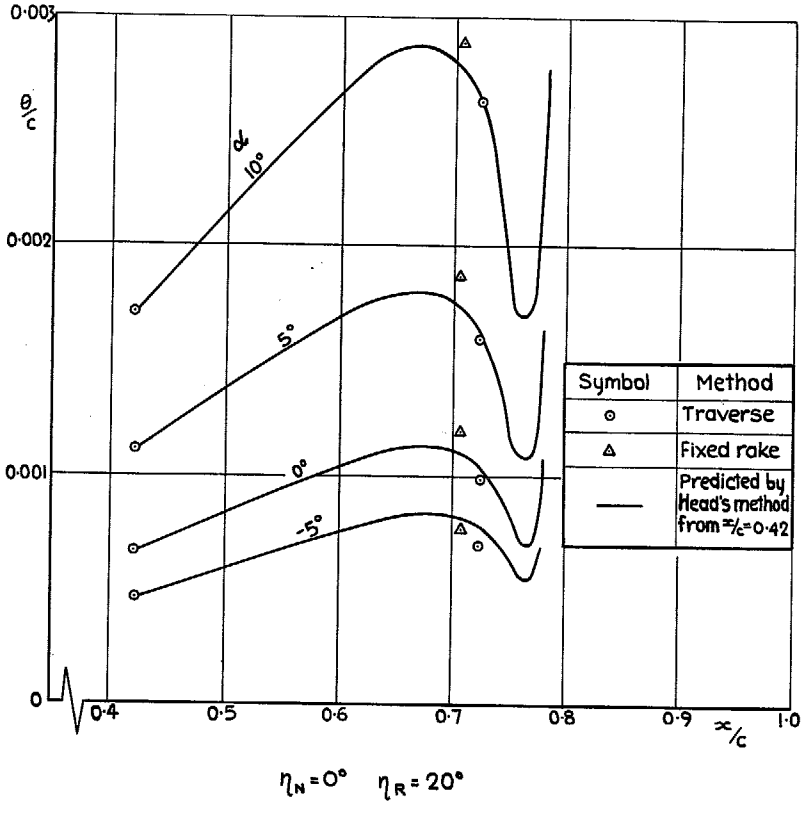

FIG. 31. Comparison of predicted and experimental boundary-layer development.

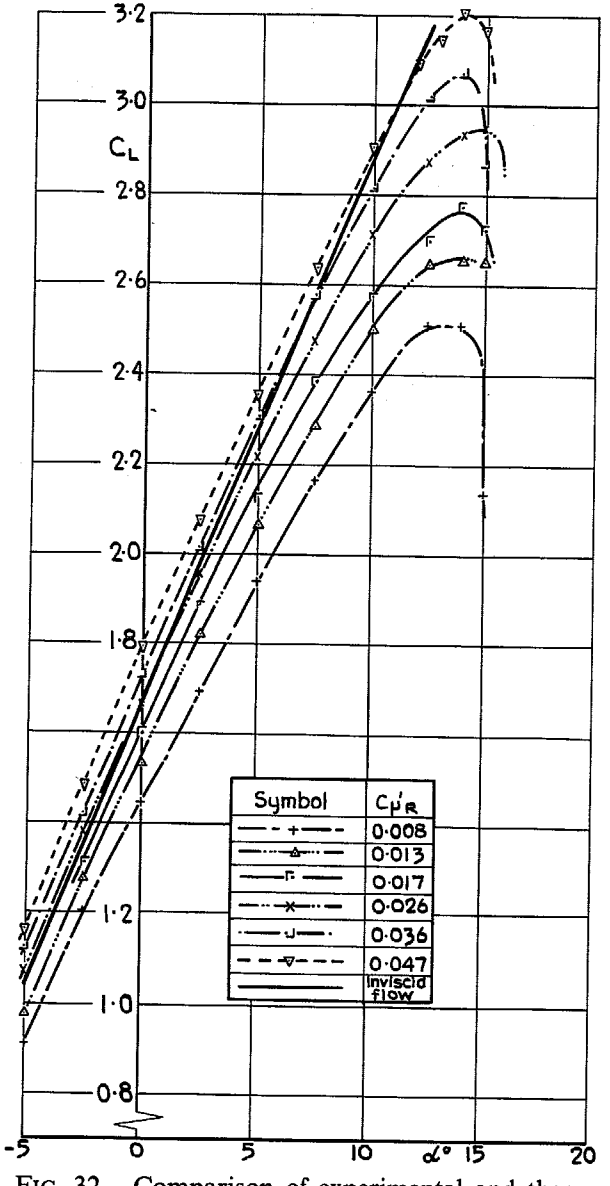

FIG. 32. Comparison of experimental and theoretical effect of angle of incidence on lift. $\eta_N = 0°, \eta_R = 20°$.

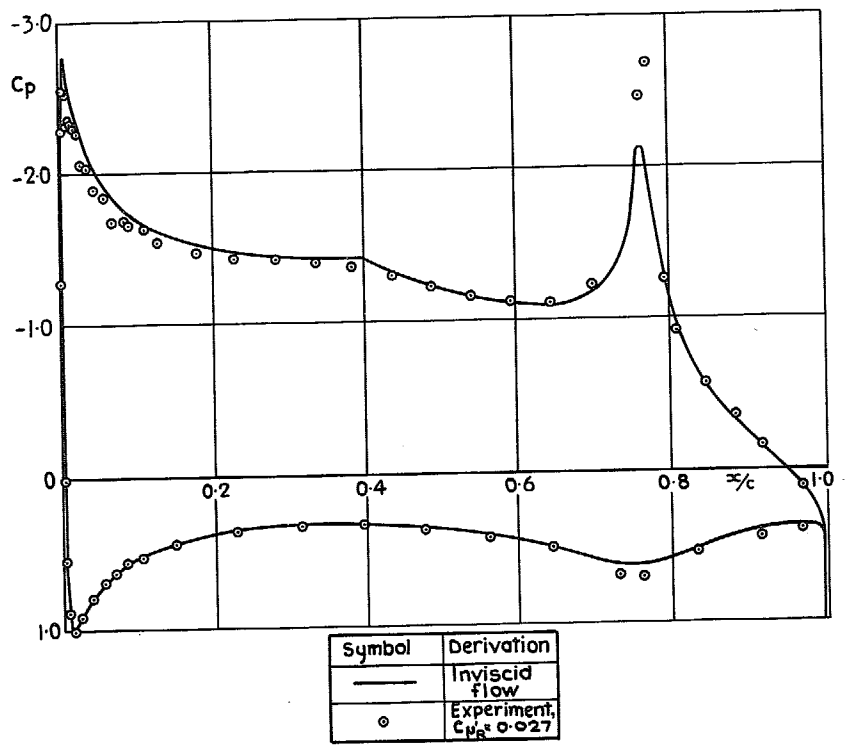

FIG. 33. Comparison of measured and predicted pressure distributions at $\alpha = 0°, \eta_N = 0°, \eta_R = 20°$

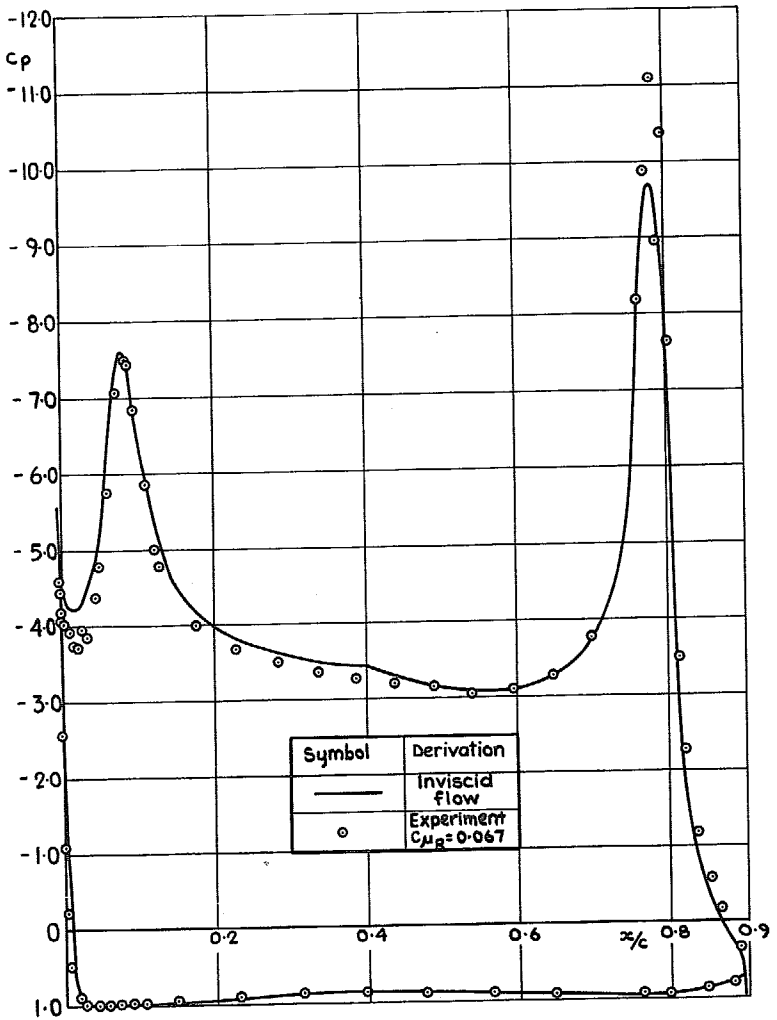

FIG. 34. Comparison of measured and predicted pressure distributions at $\alpha = 0°, \eta_N = 30°, \eta_R = 60°$

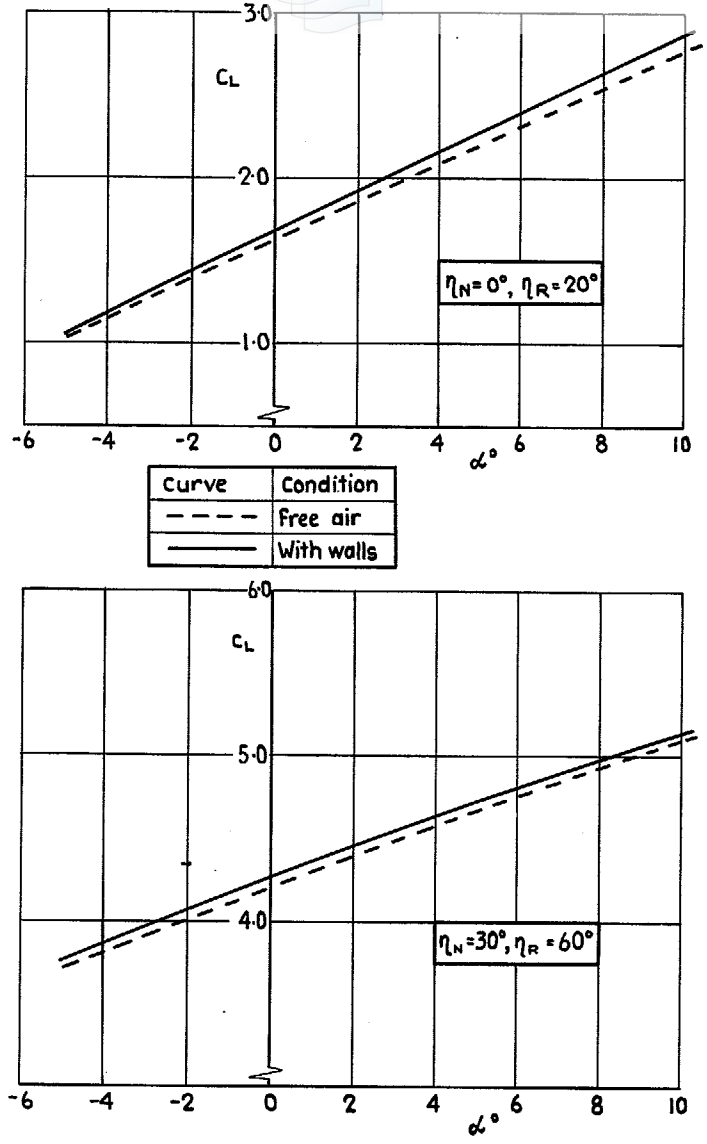

FIG. 35. Inviscid lift coefficients, with and without tunnel wall effects.

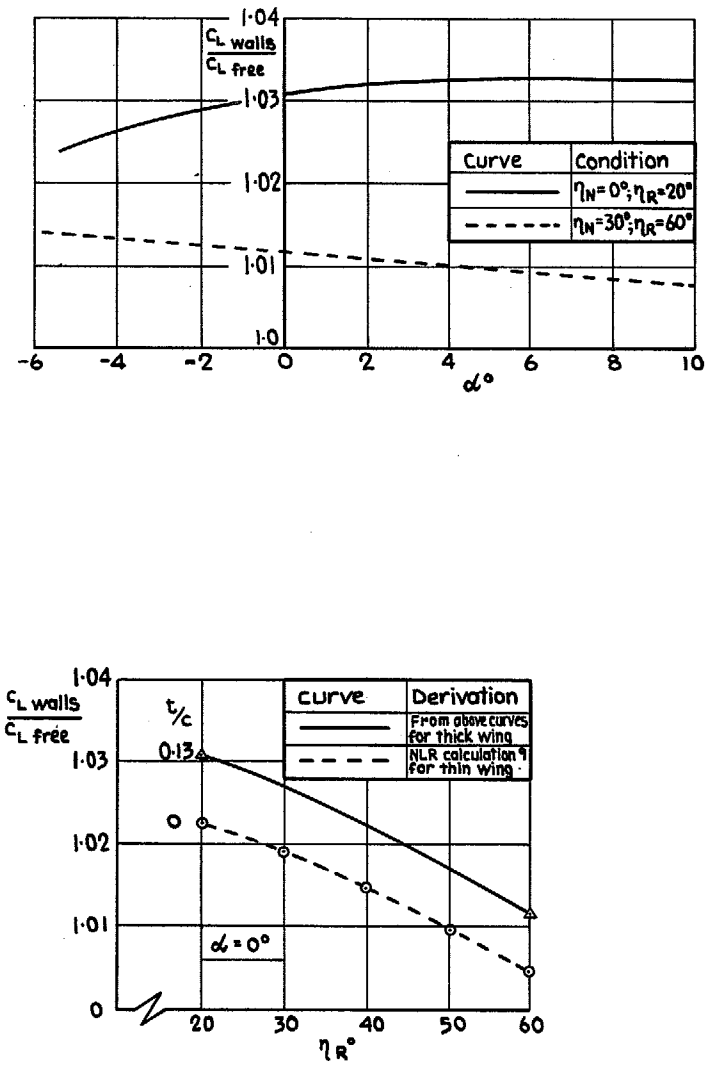

FIG. 36. Effect of angle of incidence and flap deflection on tunnel wall effect.

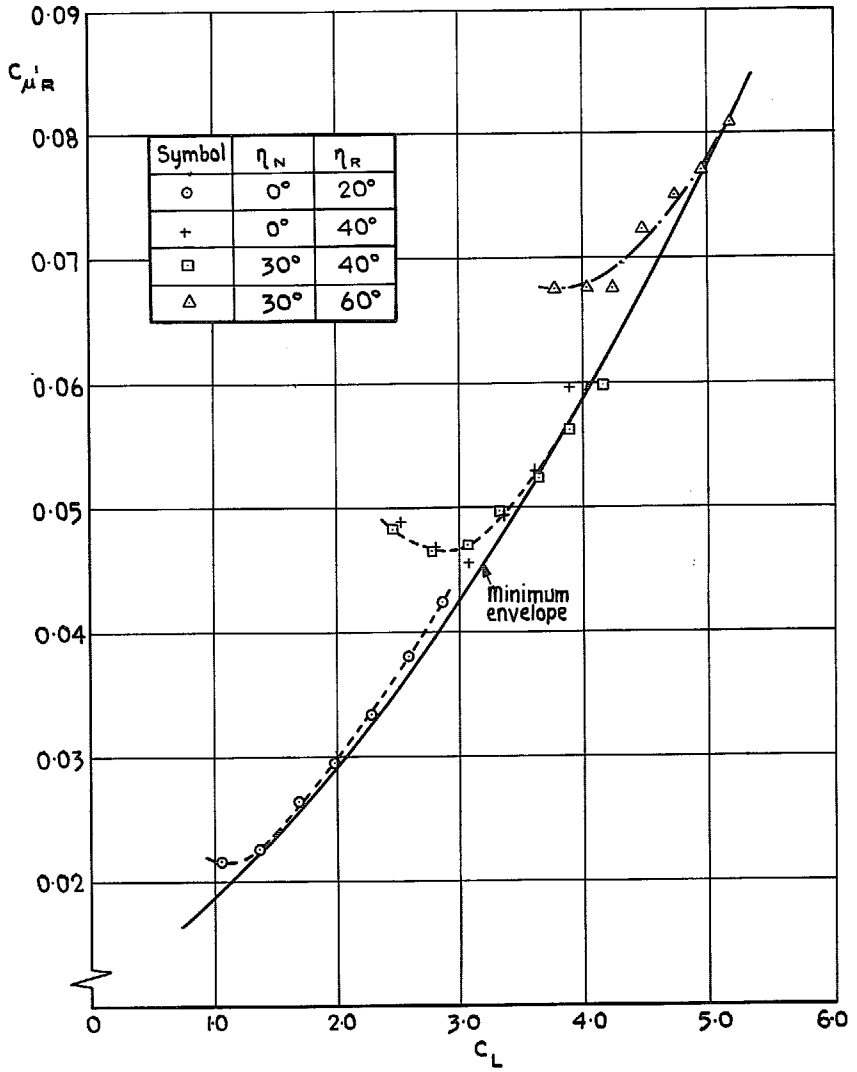

FIG. 37. Blowing momentum coefficient required to achieve the inviscid lift.

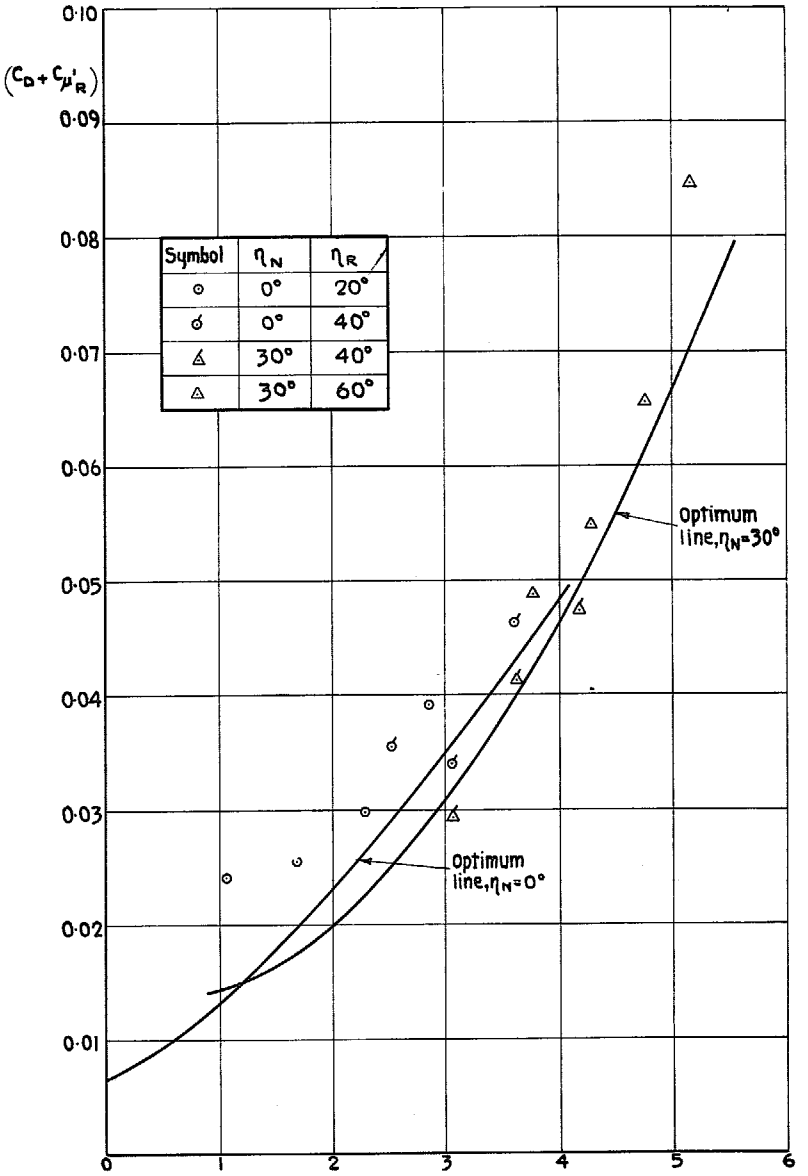

FIG. 38. Wake drag + blowing coefficient at inviscid lift.

Printed in Wales for Her Majesty's Stationery Office by Allens Printers (Wales) Limited
Dd. 501372 K.5

Published by
HER MAJESTY'S STATIONERY OFFICE

To be purchased from
49 High Holborn, London WC1
13a Castle Street, Edinburgh EH2 3AR
109 St Mary Street, Cardiff CF1 1JW
Brazennose Street, Manchester M60 8AS
50 Fairfax Street, Bristol BS1 3DE
258 Broad Street, Birmingham 1
7 Linenhall Street, Belfast BT2 8AY
or through any bookseller

SBN 11 470339 6